The genomic architecture of fitness is a major driver of population viability during rapid environmental change

Marty Kardos[1*], Gordon Luikart[1]

[1]University of Montana
Division of Biological Sciences
Flathead Lake Biological Station
32125 Biostation Lane
Polson, MT 59860, USA

*Correspondence to: marty.kardos@mso.umt.edu

Keywords: Adaptation, conservation genomics, evolution, extinction, natural selection, quantitative genetics

ABSTRACT

The rapid global loss of biodiversity calls for a robust understanding of how populations will respond demographically to environmental change. The viability of many populations will depend on their ability to adapt to rapidly changing environmental conditions. Heritability of traits under selection is known to affect the efficacy of adaptation. However, the effects of the genetic architecture underlying the heritability of selected traits (e.g., the number and effect sizes of the causal loci) on population viability remain poorly understood. We found from a wide range of deterministic theoretical models and individual-based simulations of divergent life histories (approximating corals and large mammals) that the genetic architecture of a selected trait can strongly affect population viability during selection associated with a rapidly shifting phenotypic optimum. Polygenic architectures (i.e., many loci, each with a small phenotypic effect) appear to confer greater adaptation and higher population viability than genetic architectures including large-effect loci responsible for 50-90% of the initial heritability of selected traits. Our results also suggest that the viability of populations with large-effect loci can depend strongly on initial allele frequencies, with already-frequent and very rare positively-selected alleles conferring low adaptive potential and viability compared to moderately low large-effect allele frequencies. These results uncover a crucial role of the genetic architecture underlying the heritability of fitness traits in determining eco-evolutionary dynamics and population viability during rapid environmental change.

INTRODUCTION

One of the most urgent undertakings for science and society is to understand how biodiversity will respond to human-driven environmental changes that threaten the persistence of numerous taxa globally[1-4]. Predicting if populations are likely to adapt and respond demographically to selection imposed by environmental change (e.g., global warming) is a difficult task, but crucial to understanding and mitigating the ongoing extinction crisis [2,3,5-8]. Higher heritability (h^2, the proportion of phenotypic variance arising from additive genetic effects) is known to confer increased adaptation per generation. Measuring h^2 is therefore key to understanding how populations are likely to respond to environmental change[2,4,6,9-11]. However, the influence of the number, distribution of effect sizes, and allele frequencies of loci underlying the h^2 of selected traits (i.e., the genetic architecture) on demographic responses to selection remains poorly understood.

How does the genetic architecture underlying the h^2 of a selected phenotype affect population viability? This question is timely because recent advances in genomics make it feasible, though still challenging[12], to dissect the genetic architecture of phenotypes. Recent studies show that while many fitness-related traits are highly polygenic (affected by many loci, each with a small effect)[13], many others, including traits likely to affect adaptation to climate change[14], are governed by loci with very large phenotypic effects[14-21]. Such large-effect loci are often thought to facilitate rapid adaptation[22-24]. Indeed, the initial steps of adaptation usually occur via fixation of beneficial alleles with the largest effect sizes[25]. Large-effect loci may therefore facilitate the maintenance of large population sizes through bouts of rapid environmental change. However, basic quantitative genetics theory predicts higher evolutionary potential for polygenic traits (Figure S1), and that h^2 and the rate of adaptation decline more rapidly for traits with large-effect loci than for polygenic traits[26,27]. Populations with polygenic selected phenotypes may therefore

be more likely to adapt to new conditions, and maintain larger and more viable populations, than when large-effect loci are responsible for much of the h^2.

Our objective was to determine how the genetic architecture underlying the h^2 of a selected phenotype affects the viability of populations subjected to a shifting optimal phenotype caused by rapid environmental change. Importantly, we did so while controlling for the h^2 of the selected trait at the onset of selection (h_0^2), and allowing h^2 to fluctuate through time as the underlying allele frequencies evolve. We considered a wide range of scenarios including divergent life histories, h^2 ranging from 0.4 to 0.8, initial beneficial allele frequencies from 0.05 to 0.95, and a range of gene flow rates. We also quantified effects of linkage along chromosomes, a stochastic temporal increase in the optimum phenotype, and phenotypic plasticity. To address these objectives, we used both deterministic analytical models and stochastic individual-based simulations.

RESULTS

An analytical model of evolutionary and demographic responses to environmental change

We first report results from a deterministic analytical model of selection on a quantitative trait and density-dependent population growth in a sexually reproducing species with discrete generations. This builds upon previous quantitative genetic, evolutionary-demographic models used to investigate the prevention of extinction via evolutionary rescue[9,10,28,29] (model details are in the Materials and Methods). We use this model to determine expectations for phenotypic evolution and population growth under a range of simple genetic architectures with purely additive phenotypic effects, unlinked loci, and no epistasis or plasticity, as described below. We then apply individual-based simulations to determine the effects of genetic architecture under more complex (and perhaps more realistic) scenarios.

We iterated our deterministic model for 80 generations to evaluate the effects of the number of loci underlying h^2 on the evolutionary and demographic responses to a sudden shift in the optimum phenotype due to an environmental change. We first considered simple cases where there was either one or two large-effect loci, or a large number of loci with small and equal effects responsible for the additive genetic variance of the phenotype (V_G). The populations are assumed to have an initial mean phenotype ($\bar{z}_0$) equal to its initial optimum value (θ_0), which shifts permanently to a new value of θ_1 in the first generation. We assume $h_0^2 = 0.6$, and that each of n = 1, 2, or 100 loci contributed equally to the V_G. We also assume that both $\bar{z}_0$ and θ_0 = 100 (in arbitrary units), $\theta_1 = 110$, the initial population size was $N_0 = 0.5 \times K$ (where K is the carrying capacity), and the initial frequency of positively-selected alleles at each of n loci was p_0 = 0.1, 0.3, 0.5, 0.7, or 0.9. Note that this model, and the models below, control for the initial evolvability (mean-scaled additive genetic variance)[30] in addition to h_0^2.

Results from this model suggest that the genetic architecture underlying the h^2 of a selected trait can strongly affect the evolutionary and demographic responses to a rapid environmentally-induced shift in θ. First, phenotypic evolution and population growth after the onset of selection were highly dependent on the p_0 of large-effect alleles, but relatively insensitive to p_0 when many small-effect loci were involved (Figure 1). For example, populations with a single large-effect locus and $p_0 \geq 0.5$ were predicted to decline precipitously towards extinction while N eventually

approached K in populations with $p_0 < 0.5$. The time to reach $N \approx K$ was approximately 60 generations longer when there was a single large-effect locus and $p_0 = 0.3$ compared to $p_0 = 0.1$ (Figure 1A). With 2 large-effect loci, the expected time to reach $N \approx K$ was nearly identical for $p_0 = 0.1$ and $p_0 = 0.3$. Populations with 2 large-effect loci were predicted to recover slowly with $p_0 = 0.5$, and to decline towards extinction with $p_0 > 0.5$ (Figure 1B). However, for populations with a polygenic selected trait, the expected rate of adaptation and population recovery was much less affected by p_0, with the phenotype approaching θ_1, and N approaching K under all values of p_0 (Figure 1C). Results from analyses of this model with $h_0^2 = 0.4$ and $h_0^2 = 0.8$ agree qualitatively with the results presented here (Figures S2, S3). These results suggest that large-effect loci confer adaptation and demographic recovery from selection that is similar or higher than with a polygenic architecture only when the positively-selected alleles are initially infrequent ($p_0 \approx 0.1 - 0.3$). Additionally, this model suggests that predictions of demographic responses to environmental change will be more reliable when the selected trait(s) is polygenic as doing so does not require precise estimates of the underlying allele frequencies.

While the deterministic model above is useful for understanding population responses to selection, it makes some assumptions that are unlikely to hold in natural populations. For example, the model assumes the absence of selection-induced linkage disequilibrium. Linkage disequilibrium (LD) among loci affecting a selected phenotype could be substantial, and may affect the pace of adaptation when multiple loci are involved and locus-specific selection coefficients are large[31]. The model (and previous similar models) also assumes that the selected phenotype is normally distributed. However, strong selection and/or large-effect loci can skew the phenotype distribution away from normality[31]. We therefore repeated the above analyses, implementing an explicit simulation-based model of genotype and the phenotype distributions and found that the results were not substantively different from those described above (Figure S4).

Stochastic, individual-based simulations of evolutionary and demographic responses environmental change

We developed an individual-based simulation model to account for the effects of stochasticity on phenotypic evolution (i.e., genetic drift) and demography on responses to environmentally-induced phenotypic selection (see Materials and Methods). We retain the assumptions of random mating, viability selection, and homogeneous initial allele frequencies and effect sizes across all of the loci underlying V_G. We model individual phenotypes as a function of additive effects at the underlying loci plus random environmental effects. Mates are paired at random, and the number of offspring is assumed to be Poisson distributed with a mean of $\bar{n}_o = 4$ offspring (arbitrarily). Initial population sizes were set arbitrarily to 500 with a carrying capacity of $K = 1{,}000$. We calculated the extinction rate each generation as the proportion of 500 replicate simulated populations with fewer than 2 individuals remaining.

Similar to the deterministic model results in the previous section, the lowest initial positively-selected, large-effect allele frequency ($p_0 = 0.1$) conferred substantially increased adaptation, recovery of N, and a lower extinction rate compared to large-effect alleles with higher p_0 (Figure 2A, 2B). The polygenic architecture resulted in lower extinction rate and larger N on average compared to the large-effect genetic architectures for all p_0 values except $p_0 = 0.1$, in which case the large-effect genetic architecture resulted in faster phenotypic and demographic responses to

selection (along with lower extinction rates) than the polygenic architecture. We repeated the analysis of this individual-based simulation model using lower and higher initial heritability ($h_0^2 = 0.4$ and 0.8), and the results agreed qualitatively with those for $h_0^2 = 0.6$ (Figure S5, S6, S7, S8).

The analyses above assumed that all of the positively-selected alleles conferring a larger phenotype have the same p_0 and equal phenotypic effects. A more realistic situation is likely where a selected phenotype is governed by both large- and small-effect loci across a wide range of initial allele frequencies. We therefore used our individual-based simulations to evaluate the effects of genetic architecture on population responses to selection when both large- and small-effect loci were present. We again assumed that the selected phenotype is affected by additive genetic effects at 100 loci. One of the 100 loci was responsible for between 50% and 90% of the genetic variance, with the other 99 loci contributed the remaining additive genetic variance. For each of 500 independent simulation repetitions, the frequency of the positively selected large-effect allele was drawn at random from a uniform distribution ranging from 0.05 to 0.95. We set these p_0 limits to avoid extremely large phenotypic effects (i.e., extreme values of a) at the large-effect loci. The p_0 at the 99 small-effect loci were drawn at random from a beta distribution with parameters α and β each set to 0.5, which results in a typical U-shaped allele frequency distribution where most loci had the minor allele at low frequency, as expected at mutation-drift equilibrium[32] [p. 147]. We parameterized the simulations to be informative of evolutionary and population dynamics for species with life histories typical of large mammals[33] (high survival and low fecundity) and corals[34] (low survival and high fecundity) to determine if life history strategy affected the results. We assumed $N_0 = 500$ and $K = 1{,}000$, and $N_0 = 10{,}000$ and $K = 20{,}000$ for simulations assuming approximate large mammal and coral life histories, respectively.

These simulation results are similar to the results from the simpler models presented above, with the very large-effect alleles conferring lower adaption, smaller population sizes, and a higher extinction rate on average than when the selected trait was polygenic (Figure 3). For example, the extinction rate at generation 80 was 2.0 times higher with the large-effect locus (64% extinction rate) compared to the polygenic architecture (32% extinction rate) in simulations assuming a large mammal life history. Similarly, the extinction rate was 2.7 times higher among populations with a large-effect locus (72% extinction rate) compared to the polygenic architecture (27% extinction rate) in simulations assuming a coral-like life history.

We ran 1,500 additional simulation repetitions with a large-effect locus and 99 small-effect loci affecting the selected phenotype to determine how p_0 of a large-effect locus affected population dynamics (Figure 4). These results suggest that p_0 strongly affects population dynamics. The final population sizes were highest for both life histories when p_0 was ~0.1-0.2. The lower population growth with $p_0 < 0.1$ is likely caused by rare, positively-selected alleles frequently being lost to genetic drift as the populations rapidly declined due to selection. The weaker evolutionary and demographic response in populations with already-frequent, large-effect positively selected alleles resulted in lower population growth rates and eventual extinction in a large fraction of populations with $p_0 > 0.2$. Strikingly, all of the populations with a coral life history and $p_0 > 0.5$ went extinct by generation 80.

We tested whether similar effects of genetic architecture held across a range of alternative scenarios by varying the parameters in our simulation models. We simulated lower and higher initial heritability (h_0^2=0.4 and 0.8), gene flow from a population with a different (stationary) phenotypic optimum, weaker effect sizes at large-effect loci, a stochastic linear temporal increase in the phenotypic optimum[10] (instead of a sudden shift as above), and plasticity in the selected phenotype. Polygenic architectures generally conferred substantially higher population viability on average compared to architectures including large-effect loci in all of these scenarios (Figs. S6-S13). However, the increased evolutionary and demographic responses to selection associated with polygenic architecture was smaller when there was immigration, and when the large-effect loci contributed a smaller fraction of the h^2. For example, the extinction rate was only 1.38 times higher with a large effect locus than for the polygenic architecture (compared to a 2-fold difference in the simulations of closed populations above) when there were 4 immigrants per generation from a population where the phenotypic optimum did not shift in the first generation (Figure S9, see also Figure S10 for similar results with 8 immigrants per generation). Additionally, the extinction rate among populations with a large-effect locus explaining only 50% of h^2 was 1.28 times higher than with a polygenic architecture (Figure S11).

DISCUSSION

Our results suggest a crucial role of the genetic architecture of fitness in adaptation and population viability in rapidly changing environments. It has long been known that populations with heritable genetic variation for selected traits are expected to adapt to new conditions. However, our results suggest that the characteristics of the genetic architecture underlying heritability at the onset of selection can strongly affect population viability during rapid environmental change. When loci with large phenotypic effects are present, the initial frequency of large-effect beneficial alleles can strongly affect population responses to selection. Polygenic architectures on average conferred higher evolutionary potential, more consistent evolutionary responses to selection, and increased population viability compared to when the selected trait was governed in part by a large-effect locus. Additionally, while understanding how wild populations will respond to ongoing rapid environmental change remains a difficult task, the models and results presented here may inform future efforts to understand eco-evolutionary dynamics and the extent of the ongoing extinction crisis.

The influence of genetic architecture on variation in population responses to environmental change will depend on how often fitness traits have loci with large enough effects to substantially influence the temporal dynamics of h^2 during bouts of adaptation. Recent results from several taxa, including mammals[15-18], salmonids[14,19], and birds[20,21] suggest that very large-effect alleles often influence fitness-related traits. Interestingly, seemingly complex fitness-related traits that are often assumed to be polygenic, such as horn size (a sexually-selected, condition-dependent trait)[15], migration timing[14], and age at maturity[19], have in some cases turned out to be driven almost entirely by variation at individual loci. It is therefore crucial to quantify the effect sizes and allele frequencies at loci with large effects when they are present in systems where future eco-evolutionary dynamics are of interest.

It can be difficult to predict or measure the frequency of alleles with large beneficial effects under rapid environmental change. For example, large-effect alleles for traits subjected to

historical balancing selection are likely to be at intermediate frequencies [35]. Recent large-effect mutations are likely to be found at low frequencies. Previously neutral or nearly-neutral alleles that affect fitness in new conditions are likely to be found across the entire spectrum of allele frequencies. Fortunately, increasingly efficient DNA sequencing and improving approaches for conducting genotype-phenotype association analysis provide the tools necessary to estimate h^2, and to identify large-effect loci (and to estimate their allele frequencies) where they exist[7,36].

Why do polygenic architectures usually confer increased population viability compared to genetic architectures including large-effect loci? This finding appears to arise in part from a slower and less variable decline in h^2 during adaptation for polygenic traits than for traits with large-effect loci (Figures S2, S3, S4, S5)[26]. The rapid decline in h^2 when large-effect beneficial alleles are already common, and the frequent loss of initially rare large-effect alleles means that there is a narrow window of p_0 where traits with large-effect architectures are likely to evolve in response to selection as fast or faster than polygenic traits. Additionally, evolutionary and demographic responses to selection were more stochastic in populations with large-effect loci (Figures 3). This suggests that reliably predicting population responses to selection is more difficult when large-effect loci are present, particularly if the initial frequency of large effect alleles is not known precisely. Specifically, these results highlight the importance of identifying large-effect loci where they exist, and using information on their effect-sizes and allele frequencies along with h_0^2 in models predicting demographic responses to environmental change. Predictions of population responses to selection that do not account for the strong effects of genetic architecture on the temporal dynamics of h^2 and adaptation are likely to be misleading.

Understanding how populations will respond to environmental change is both challenging and vitally important in conservation and evolutionary ecology[2]. Reliable predictions of how biodiversity will respond to large-scale environmental change are necessary to efficiently prioritize scarce conservation resources and to develop effective strategies to conserve populations, and to mitigate inevitable biodiversity losses. However, there are considerable obstacles to reliably predicting responses to selection. For example, the complex and interacting effects of environmental stochasticity, genotype-by-environment interactions, phenotypic plasticity, pleiotropy, dominance interactions, gene flow, simultaneous selection on multiple potentially correlated traits, and changing community structure (i.e., species interactions) could all strongly affect adaptation and population dynamics, but are also difficult to measure and to forecast into the future. It will often be difficult to reliably predict how wild populations will respond to large-scale environmental change. We therefore encourage caution when attempting to predict eco-evolutionary dynamics under climate change and other human-driven environmental changes.

Our results uncover a likely widespread phenomenon where, for a given h^2 starting condition, polygenic architectures can often confer higher average adaptive potential and increased population viability under rapidly shifting phenotypic optima compared to genetic architectures with large-effect loci. Incorporating these effects of genetic architecture into population viability models could substantially advance understanding of the consequences of human-driven environmental change for species survival and biodiversity conservation. Improved understanding of vulnerability to environmental change could also advance strategies to conserve

vital natural and agricultural resources[7,37,38], for example by identifying populations and species to prioritize for conservation action.

MATERIALS AND METHODS

An analytical model of eco-evolutionary dynamics

We model diploid populations that have discrete generations and follow a discrete logistic model[39] of density-dependent population growth. Individual fitness is modeled as a Gaussian function of a quantitative trait, such that the fitness of an individual with phenotype value z is

$$W(z) = W_{\max} e^{\frac{(z-\theta)^2}{2c^2}}, \qquad (1)$$

where $W_{\max}$ is the fitness of an individual with optimum phenotype value θ when the population size $N \to 0$, and c^2 defines the width of the fitness function. The population is assumed to have an initial mean phenotype of $\bar{z}_0$ equal to the initial phenotypic optimum θ_0. The selected phenotype is assumed to be normally distributed with additive genetic (V_G) and random environmental (V_E) variance components summing to the total phenotypic variance V_z ($h^2 = V_G / V_z$). The phenotype's probability density function is therefore

$$P(z) = \frac{1}{\sigma_z \sqrt{2\pi}} e^{-\frac{(z-\bar{z})^2}{2V_z}}, \qquad (2)$$

where $\bar{z}$ is the mean phenotype value in the population, σ_z is the phenotype standard deviation. $\bar{z}$ is calculated as

$$\bar{z} = \theta_0 - \bar{G}_0 + n \frac{\sum_{i=1}^{3} f_i' g_i}{\sum_{i=1}^{3} f_i'}, \qquad (3)$$

where $\bar{G}_0$ is the mean additive genetic value in the first generation, f_i' is the frequency of the i^{th} of the three possible diploid genotypes, and g_i is the genetic value of the i^{th} of the three possible genotypes. A sudden environmental change permanently shifts θ from its initial value θ_0 in the first generation to θ_1, thus imposing directional selection on the phenotype and an environmental challenge to the persistence of the population.

We assume that the allele conferring a larger phenotype (the A1 allele) has the same initial frequency p_0 at each of n biallelic loci. Further, the frequency of the A1 allele(s) is assumed to evolve identically at each of the n loci, such that p in generation $t + 1$ at each locus is

$$p_{t+1} = \frac{p_t \bar{w}_{11} + p_t(1-p_t)\bar{w}_{12}}{\bar{w}_t}, \qquad (4)$$

where $\bar{w}_{11}$ and $\bar{w}_{12}$ represent the mean relative fitness of homozygous A1A1 genotypes, and heterozygous A1A2 genotypes, respectively, and $\bar{w}_t$ is the mean individual fitness in generation t. Mean individual fitness in the population is calculated by integrating over the product of the fitness and phenotype density functions:

$$\bar{w} = \int W(z)P(z)\,dz. \qquad (5)$$

The mean genotype-specific relative fitness (i.e., $\bar{w}_{11}$ or $\bar{w}_{12}$) is calculated as in (5) except with the variance (V_z) and mean ($\bar{z}$) of the phenotype probability density function being conditional on holding the genotype constant at a locus. The V_z conditional on holding the genotype constant at a locus is

$$V_{z,C} = \sum_{i=1}^{n-1} 2p(1-p)a^2 + V_E, \qquad (6)$$

where a is half the phenotypic difference between the two alternative homozygous genotypes. The mean phenotype conditional on holding the genotype constant at a locus is

$$\bar{z}_g = \theta_0 - \bar{G}_0 + g' + (n-1)\frac{\sum_{i=1}^{3} f_i' g_i}{\sum_{i=1}^{3} f_i'}, \qquad (7)$$

where g' is the genetic value of the single-locus genotype being held constant (i.e., $g' = 0$ for genotype A2A2, $g' = a$ for A1A2, and $g' = 2a$ for A1A1), f_i' is the frequency of the i^{th} of the three possible diploid genotypes, and g_i is the genetic value of the i^{th} of the three possible genotypes. The first two terms in (7) center the phenotype distribution at θ_0 in the first generation. The mean genotype-specific fitness [i.e., $\bar{w}_{11}$ and $\bar{w}_{12}$ in (4)] is calculated as in (5), after first replacing $\bar{z}$ and V_z with $\bar{z}_g$ and $V_{z,C}$ in (2).

We calculate h^2 each generation as

$$h^2 = \frac{\sum_{i=1}^{n} 2p_i(1-p_i)a^2}{V_p}. \qquad (8)$$

Population size (N) in generation $t + 1$ is calculated following a discrete logistic model of population growth as

$$N_{t+1} = N_t e^{\left(\ln(\bar{w}_t)\left[1-\frac{N_t}{K}\right]\right)}, \qquad (9)$$

where K is the carrying capacity.

An individual-based simulation model of eco-evolutionary dynamics

Our model simulates populations with stochastic, density-dependent population growth and viability selection on a quantitative trait. The simulations began by initializing the population with N_0 individuals in generation one. Genotypes at 100 unlinked, diallelic SNPs for the N_0 individuals were drawn at random from the specified initial allele frequency (p_0) distribution. p_0 was either held constant across all loci (e.g., for data shown in Figure 2), or sampled from a beta distribution with shape parameters of $\alpha = 0.5$ and $\beta = 0.5$ (e.g., for the data presented in Figure 3). These beta distribution parameters produced a U-shaped allele frequency distribution where most loci had low minor allele frequencies, as expected at mutation-drift equilibrium [32] [p. 147].

For simulations with a large-effect locus responsible for 50%, 70%, or 90% of h_0^2, we selected the large-effect locus at random from the 100 SNPs, and assigned the additive genetic variance

for this locus as, for example, $2pqa^2 = 0.9V_G$ (for the case where the large-effect locus was responsible for 90% of V_G), where a is the allelic effect (half the average phenotypic difference between the two homozygous genotypes). The remaining phenotypic variance (V_E) was attributed to random environmental differences among individuals ($V_E = V_z - V_G$, $V_G = h^2V_z$). Each small-effect locus was assumed to contribute the same additive genetic variance to the selected phenotype. The simulations then iterated through the following sequence of events (*SI Appendix* Fig. S16) until either extinction or 100 generations.

Simulating the selected phenotype

We assumed that the selected phenotype had an initial variance of $V_z = 10$. Individual i's phenotype was determined as

$$z_i = \theta_0 - \bar{G}_0 + \sum_{j=1}^{n} c_{ji}\, a_j + \varepsilon_i, \qquad (10)$$

where θ_0 is the specified mean phenotype in the first generation, $\bar{G}_0$ is the mean additive genetic value among individuals in the first generation, c_{ji} is individual i's count of the allele conferring a larger phenotype at the jth locus, and a_j is the allelic effect at the jth locus, at n SNPs, and the environmental effect ε_i is drawn at random from a normal distribution with mean=0 and variance=V_E. We assume no dominance or epistatic effects.

Fitness as a function of phenotype

Each population was subjected to viability selection on the simulated phenotype. The expected (deterministic) fitness (w) for each individual in generation t was calculated as in equation (1) above. The mean deterministic fitness in generation t ($\bar{w}_t$), N_t, and K were applied to equation (9) to find the deterministic expected population size in generation $t + 1$ ($N_{exp,t+1}$, the total expected number of offspring left by generation t). The survival probability of each individual in generation t was then calculated as

$$\bar{s} = \frac{N_{exp,t+1}}{N_t \bar{n}_o}. \qquad (11)$$

The number of individuals in generation t surviving to maturity was calculated as

$$N_{s,t} = \sum_{i=1}^{N_t} r_i \begin{cases} 0 & \text{if } R_i > \bar{s} \\ 1 & \text{if } R_i \leq \bar{s}, \end{cases} \qquad (12)$$

where R_i is a number selected at random from a uniform distribution bounded by 0 and 1 (using the *runif* function in R). $N_{s,t}$ individuals surviving to maturity in generation t are then selected at random (using the *sample* function in R) from N_t individuals, with sampling weight w, such that individuals with w closer to θ_1 are more likely to survive to maturity.

Mating and meiosis

Mates were paired at random with no self-fertilization allowed. The number of offspring per family was Poisson distributed, with mean of 4 offspring for simulated mammal populations ($r_{max} = 0.41$), and 26 offspring for coral populations ($r_{max} = 0.26$). Each offspring inherited gene

copies from the parents following Mendelian probabilities. We assumed unlinked loci (i.e., free recombination among all pairs of loci).

Note simulation-based and analytical approaches above control for the initial evolvability (mean-scaled additive genetic variance)[30] in addition to h_0^2. The R packages implementing the deterministic and simulation models above, along with example scripts are freely available (https://github.com/martykardos/geneticArchPopDynamics).

Statistical analysis

We constructed 95% percentile bootstrap confidence intervals[40] for the proportion of extinct populations in each of our 14 simulation scenarios. The confidence intervals shown in Figures 3, S9, and S10 were constructed as follows. First, we randomly resampled 400 simulation data sets 1,000 times, with replacement, from the 400 original simulation repetitions. For each of the 1,000 bootstrap samples, we calculated the proportion of the 400 simulated populations that were extinct in each of the 100 generations. We constructed the 95% bootstrap confidence intervals for the extinction rate for each of the 100 generations as the 2.5% and 97.5% quantiles from the bootstrapped parameter distributions. The same procedure was used to construct confidence intervals for the final population sizes (N_{100}) shown in Fig. 3.

ACKNOWLEDGEMENTS

M.K. was supported by Montana Fish, Wildlife & Parks. G.L. and M.K. were supported partially by National Science Foundation grants DoB-1639014, and National Aeronautics and Space Administration grant number NNX14AB84G. We thank Fred W. Allendorf, Matthew Jones, L. Scott Mills, Alden Wright, Jeff Hard, and Robin Waples for helpful discussions and/or comments on a previous version of the manuscript.

REFERENCES

1 Mills, L. S. *et al.* Winter color polymorphisms identify global hot spots for evolutionary rescue from climate change. *Science* **359**, 1033-1036 (2018).

2 Urban, M. C. *et al.* Improving the forecast for biodiversity under climate change. *Science* **353**, aad8466 (2016).

3 Stockwell, C. A., Hendry, A. P. & Kinnison, M. T. Contemporary evolution meets conservation biology. *Trends in Ecology & Evolution* **18**, 94-101 (2003).

4 Nadeau, C. P. & Urban, M. C. Eco-evolution on the edge during climate change. *Ecography* **42**, 1-18 (2019).

5 Shaw, R. G. From the past to the future: considering the value and limits of evolutionary prediction. *The American Naturalist* **193**, 1-10 (2019).

6 Chevin, L.-M., Lande, R. & Mace, G. M. Adaptation, plasticity, and extinction in a changing environment: towards a predictive theory. *PLoS Biology* **8**, e1000357 (2010).

7 Funk, W., Forester, B. R., Converse, S. J., Darst, C. & Morey, S. Improving conservation policy with genomics: a guide to integrating adaptive potential into US Endangered

Species Act decisions for conservation practitioners and geneticists. *Conservation Genetics*, 1-20 (2018).

8 Alberto, F. J. *et al.* Potential for evolutionary responses to climate change–evidence from tree populations. *Global Change Biology* **19**, 1645-1661 (2013).

9 Gomulkiewicz, R. & Holt, R. D. When does evolution by natural selection prevent extinction? *Evolution* **49**, 201-207 (1995).

10 Lynch, M. & Lande, R. in *Biotic interactions and global change* 234-250 (United States, 1993).

11 Falconer, D. S. & Mackay, T. F. C. *Introduction to quantitative genetics*. 4 edn, (Pearson, 1996).

12 Kardos, M., Husby, A., McFarlane, S. E., Qvarnström, A. & Ellegren, H. Whole-genome resequencing of extreme phenotypes in collared flycatchers highlights the difficulty of detecting quantitative trait loci in natural populations. *Molecular Ecology Resources* **16**, 726-741 (2016).

13 Boyle, E. A., Li, Y. I. & Pritchard, J. K. An expanded view of complex traits: from polygenic to omnigenic. *Cell* **169**, 1177-1186 (2017).

14 Thompson, T. Q. *et al.* Anthropogenic habitat alteration leads to rapid loss of adaptive variation and restoration potential in wild salmon populations. *Proceedings of the National Academy of Sciences* **116**, 177-186 (2019).

15 Johnston, S. E. *et al.* Life history trade-offs at a single locus maintain sexually selected genetic variation. *Nature* **502**, 93-95 (2013).

16 Kardos, M. *et al.* Whole-genome resequencing uncovers molecular signatures of natural and sexual selection in wild bighorn sheep. *Molecular Ecology* **24**, 5616-5632 (2015).

17 Epstein, B. *et al.* Rapid evolutionary response to a transmissible cancer in Tasmanian devils. *Nature Communications* **7**, 12684 (2016).

18 Jones, M. R. *et al.* Adaptive introgression underlies polymorphic seasonal camouflage in snowshoe hares. *Science* **360**, 1355-1358 (2018).

19 Barson, N. J. *et al.* Sex-dependent dominance at a single locus maintains variation in age at maturity in salmon. *Nature* **528**, 405-408 (2015).

20 Lamichhaney, S. *et al.* Structural genomic changes underlie alternative reproductive strategies in the ruff (*Philomachus pugnax*). *Nature Genetics* **48**, 84-88 (2016).

21 Lamichhaney, S. *et al.* Evolution of Darwin's finches and their beaks revealed by genome sequencing. *Nature* **518**, 371-375 (2015).

22 Slate, J. *et al.* Genome mapping in intensively studied wild vertebrate populations. *Trends Genet* **26**, 275 - 284 (2010).

23 Dixon, G. B. *et al.* Genomic determinants of coral heat tolerance across latitudes. *Science* **348**, 1460-1462 (2015).

24 Gomulkiewicz, R., Holt, R. D., Barfield, M. & Nuismer, S. L. Genetics, adaptation, and invasion in harsh environments. *Evolutionary Applications* **3**, 97-108 (2010).

25 Orr, H. A. The population genetics of adaptation: the adaptation of DNA sequences. *Evolution* **56**, 1317-1330 (2002).

26 Walsh, B. & Lynch, M. *Evolution and selection of quantitative traits*. (Oxford University Press, 2018).

27 Barton, N. H. & Keightley, P. D. Multifactorial genetics: understanding quantitative genetic variation. *Nature Reviews Genetics* **3**, 11-21 (2002).
28 Chevin, L. M. & Lande, R. When do adaptive plasticity and genetic evolution prevent extinction of a density-regulated population? *Evolution* **64**, 1143-1150 (2010).
29 Lande, R. The response to selection on major and minor mutations affecting a metrical trait. *Heredity* **50**, 47-65 (1983).
30 Hansen, T. F., Pélabon, C. & Houle, D. Heritability is not evolvability. *Evolutionary Biology* **38**, 258-277 (2011).
31 Barton, N. & Turelli, M. Natural and sexual selection on many loci. *Genetics* **127**, 229-255 (1991).
32 Kimura, M. *The neutral theory of molecular evolution*. (Cambridge University Press, 1984).
33 Mduma, S. A., Sinclair, A. & Hilborn, R. Food regulates the Serengeti wildebeest: a 40-year record. *Journal of Animal Ecology* **68**, 1101-1122 (1999).
34 Fadlallah, Y. H. Population dynamics and life history of a solitary coral, *Balanophyllia elegans*, from Central California. *Oecologia* **58**, 200-207 (1983).
35 Llaurens, V., Whibley, A. & Joron, M. Genetic architecture and balancing selection: the life and death of differentiated variants. *Molecular Ecology* **26**, 2430-2448 (2017).
36 Yang, J., Zaitlen, N. A., Goddard, M. E., Visscher, P. M. & Price, A. L. Advantages and pitfalls in the application of mixed-model association methods. *Nature Genetics* **46**, 100-106 (2014).
37 Aitken, S. N. & Whitlock, M. C. Assisted gene flow to facilitate local adaptation to climate change. *Annual Review of Ecology, Evolution, and Systematics* **44**, 367-388 (2013).
38 Flanagan, S. P., Forester, B. R., Latch, E. K., Aitken, S. N. & Hoban, S. Guidelines for planning genomic assessment and monitoring of locally adaptive variation to inform species conservation. *Evolutionary Applications* **11**, 1035–1052 (2017).
39 May, R. M. Biological populations with nonoverlapping generations: stable points, stable cycles, and chaos. *Science* **186**, 645-647 (1974).
40 Efron, B. & Tibshirani, R. J. *An introduction to the bootstrap*. (Chapman & Hall/CRC, 1994).

AUTHOR CONTRIBUTIONS

M.K. conceived the study. M.K. and G.L. designed the study. M.K. wrote the models and simulations and analyzed the data. M.K. and G.L. wrote the paper.

FIGURES

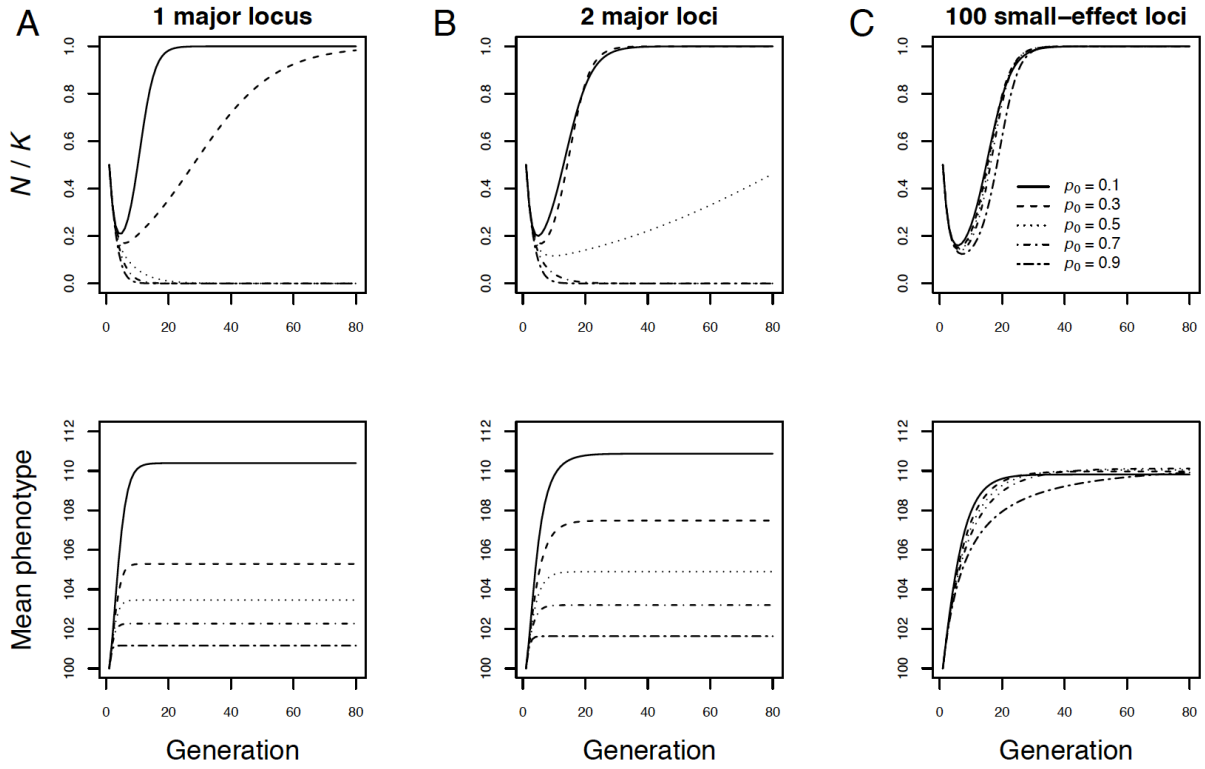

Figure 1. Deterministic analytical predictions of evolutionary (bottom row) and demographic (top row) responses to directional selection in density-regulated populations with a single large-effect locus (**A**), two large-effect loci (**B**), and 100 small-effect loci (**C**) affecting a quantitative trait under directional selection after a sudden environmental change. The y-axis in the top row shows population size (N) as a fraction of carrying capacity (K). The initial heritability was $h_0^2 = 0.6$ in all cases. Line types indicate the initial frequencies of the positively selected allele(s) conferring a larger phenotype. Initial population size was $K/2$.

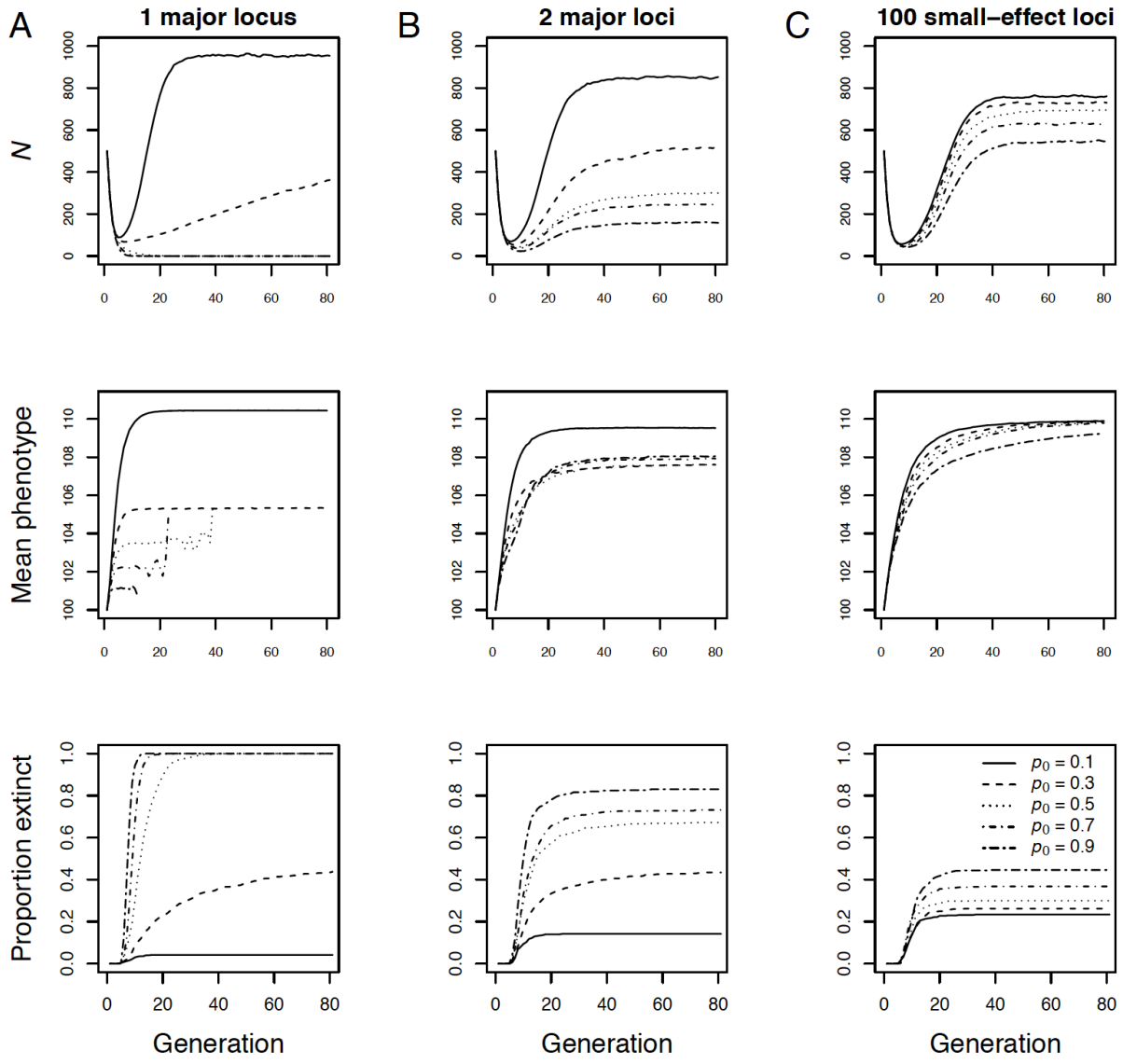

Figure 2. Individual-based simulations of evolutionary and demographic responses to directional selection in density-regulated populations with a single large-effect locus (**A**), two large-effect loci (**B**), and 100 small-effect loci (**C**) affecting a quantitative trait under directional selection after a sudden environmental change. The initial heritability was $h_0^2 = 0.6$ in all cases. Line types indicate the initial frequencies of the positively selected allele(s) conferring a larger phenotype. Initial population size was $N_0 = 500$, and varying capacity was $K = 1{,}000$.

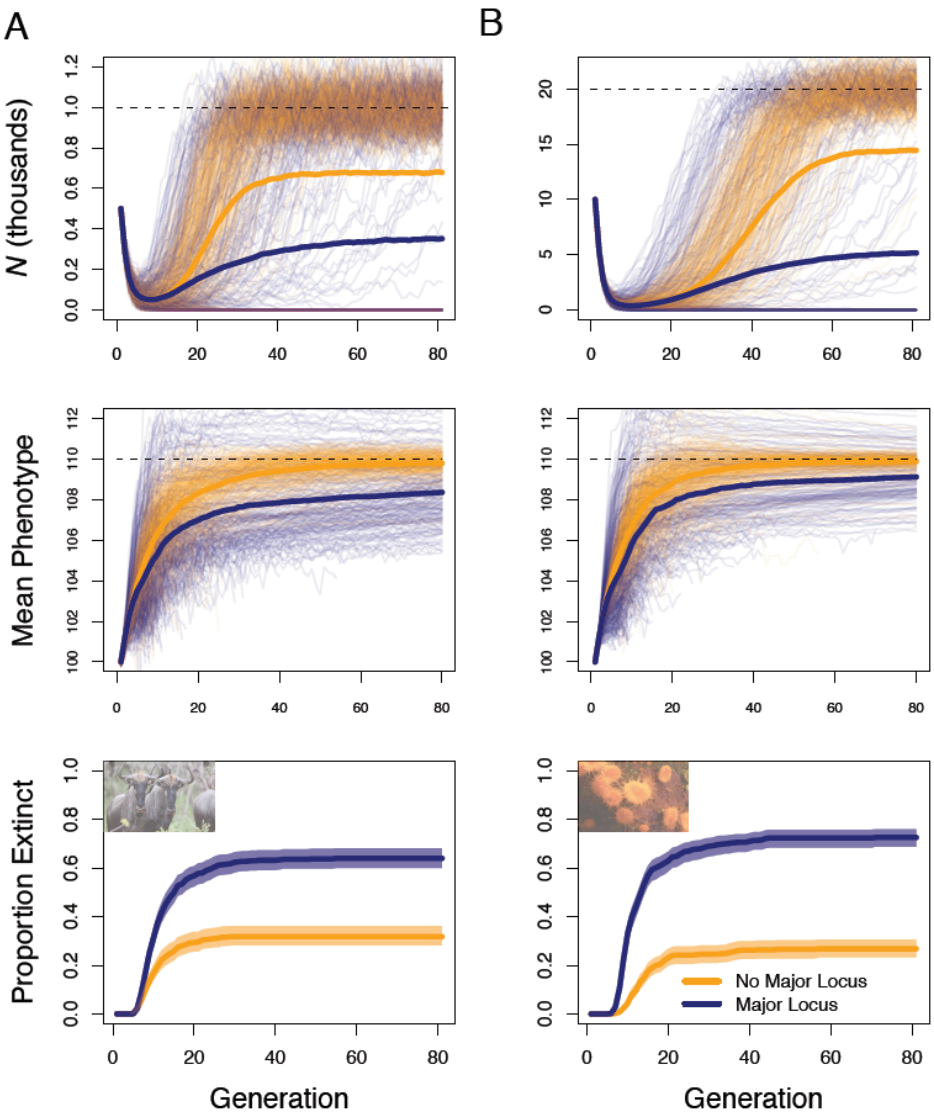

Figure 3. Effects of genetic architecture on phenotypic evolution and population dynamics in closed populations with life histories approximating large mammals (**A**), and corals (**B**). Results from populations with a large-effect locus are shown in blue; populations where the selected trait was polygenic are in orange. Thin lines show the population size (top row) and mean phenotype (middle row) through time. Thick lines show the mean population size and phenotype across all 500 repetitions. The bottom panels show the proportion of extinct populations through time, with percentile bootstrap 95% confidence intervals.

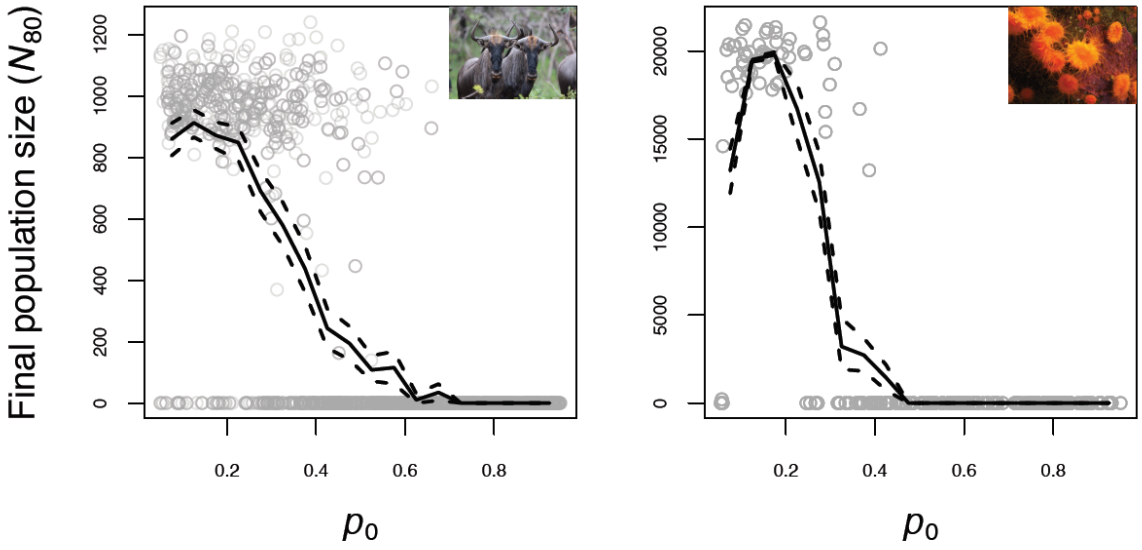

Figure 4. Effects of the initial large-effect allele frequency (p_0) on final population size in simulations with approximate large mammal (**A**) and coral (**B**) life histories. The y-axis represents the final population size at generation 80 (N_{80}), and the x-axis shows the large-effect allele p_0. The solid lines represent the mean N_{80} across 2,000 simulation repetitions in non-overlapping p_0 windows of width 0.05. Dashed lines are 95% percentile bootstrap confidence intervals for mean N_{80}.

SUPPLEMENTARY MATERIALS

The genomic architecture of fitness is a major driver of population viability in changing environments

Marty Kardos[1*], Gordon Luikart[1]

[1]University of Montana, Division of Biological Sciences, Flathead Lake Biological Station, 32125 Biostation Lane, Polson, MT 59860, USA
*Correspondence: marty.kardos@mso.umt.edu

Effects of gene flow on the influence of genetic architecture on population viability

Previous work suggests that selection with gene flow can favor the evolution of genetic architectures that have large-effect loci[1]. The presence of large-effect loci may therefore confer more robust evolutionary and demographic responses to selection when there is gene flow from populations with a different phenotypic optimum. We ran simulations equivalent to our individual-based simulations with a large mammal-like life history in the main text, except with immigration (either 4 or 8 immigrants / generation) from a population where the phenotypic optimum remained at 100 instead of shifting to 110 in the first generation.

The polygenic trait architecture conferred higher population viability in populations with immigration from a population with a different phenotypic optimum. The extinction rate was 55% among populations with a polygenic architecture, and 76% in populations with a large-effect locus when the immigration rate was four individuals per generation (Figure S9). With a higher immigration rate (8 individuals per generation), the extinction rate was 48% among populations with the polygenic architecture, and 74% in populations with a large-effect locus (Figure S10).

We then evaluated the influence of the major locus effect sizes on evolutionary and demographic responses to selection. We ran our simulations of large mammals with the large-effect locus responsible for 50%, 70% and 90% of h_0^2 and compared the results to simulations where the selected trait was polygenic. In all cases, the responses to selection were stronger for the polygenic architecture than when there was a large-effect locus. The extinction rates were 1.28, 1.84, and 2.01 times higher with large-effect loci responsible for 50%, 70%, and 90% of h_0^2, respectively, than for the polygenic architecture (extinction rate = 0.32, Figure S11).

Effects of genetic architecture on population viability with a temporally increasing and stochastic phenotypic optimum value

Our analyses in the main text of the paper focused on the simple scenario where selection is induced by a sudden and permanent environmental change. However, some environmental change is often stochastic and spread out over long periods of time. We therefore used our individual-based simulation model with a large mammal-like life history to evaluate the effects of genetic architecture on population dynamics under this type of environmental change. We ran simulations equivalent to those shown in Figure 3A in the main text, except here the phenotypic

optimum increased linearly with time (from 100 to 110) over the first *x* generations, with an error term to incorporate temporal stochasticity. The phenotypic optimum value for generation *t* was calculated as

$$\theta_t = \begin{cases} \theta_0 + \frac{t}{x}(\theta_{max} - \theta_0) + \varepsilon & \text{if } t < x \\ \theta_{max} + \varepsilon & \text{if } t \geq x \end{cases} \qquad \text{(S1)}$$

where θ_0 is the initial phenotypic optimum, θ_{max} is the final deterministic phenotypic optimum value, and ε is normally distributed with mean of zero and standard deviation of 2. We ran 500 simulation replicates with $x = 10$ generations, and also with $x = 20$ generations. The results are show below in Figure S13, and were qualitatively equivalent to those presented in Figure 3A in the main text.

Effects of genetic architecture on population viability with linked loci

Our analyses in the main text assumed that loci were unlinked. Linkage disequilibrium arising from having linked fitness-related loci can affect the response to selection[2]. We therefore ran simulations equivalent to those shown in Figure 3A, except here we placed the selected loci randomly across 10 linkage groups, each with a genetic length of 50 cM and physical length of 100 Mb, randomly selected crossover locations, and a Poisson distributed number of crossovers per meiosis. The results are shown in Figure S14 below, and were nearly identical to those in Figure 3A.

Effects of the genetic architecture on population viability with phenotypic plasticity

A previous theoretical population genetic model suggested that loci with large effects may provide higher adaptive potential and population viability when the selected phenotype is plastic[3]. We therefore tested effects of genetic architecture in the presence of phenotypic plasticity. We used a model of plasticity similar to that of Nunney[3]. We modified equation (10) from the main text to incorporate a linear effect of the optimal phenotype on the realized phenotype as

$$z_i = \theta_0 - \bar{G}_0 + \sum_{j=1}^{n} c_{ji}\, a_j + m\left(\theta_t - \left[\theta_0 - \bar{G}_0 + \sum_{j=1}^{n} c_{ji}\, a_j\right]\right) + \varepsilon_i, \qquad \text{(S2)}$$

where *m* is the rate change in expected phenotype per unit difference between the optimal phenotype and individual *i*'s expected phenotype in the absence of plasticity. The plasticity model is shown with examples in Figure S15 below. We ran 500 simulation replicates equivalent to those described above (where there is a stochastic and linear increase in θ with time) except here we considered values of $m = 0.1$, 0.2, and 0.4. The results from these simulations are consistent with the results above and in the main text (e.g., Figure 3). The polygenic architecture on average conferred higher population sizes and a lower extinction rate than when there was a large-effect locus in simulations with $m = 0.1$, and $m = 0.2$ (Figure S16). The extinction rate was <0.05 for both genetic architectures when phenotypic plasticity was strong ($m = 0.4$).

SUPPLEMENTARY FIGURES

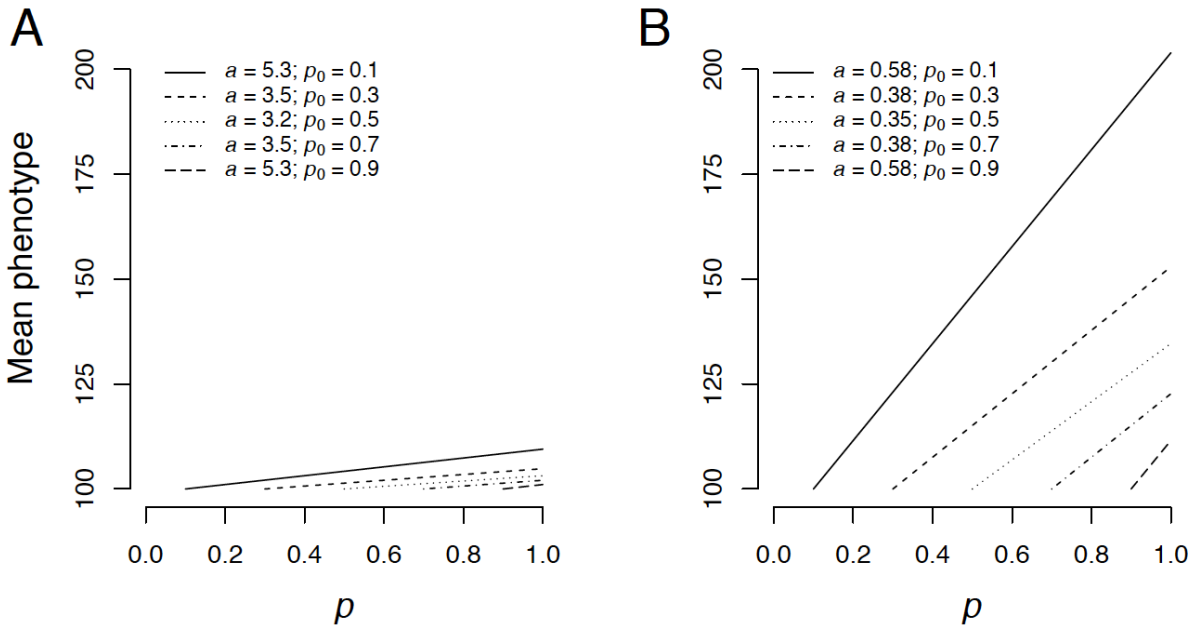

Figure S1. Evolutionary potential in populations with a single large-effect locus (**A**), and 100 small-effect loci (**B**) controlling a phenotypic trait under directional viability selection. The initial heritability was $h^2 = 0.5$ in all cases. Mating was assumed to be random and genotypes are assumed to be in Hardy-Weinberg proportions. The expectations for potential phenotypic change as the positively selected allele(s) conferring a larger phenotype go from the initial allele frequency p_0 to fixation are shown for p_0 ranging from 0.1 to 0.9.

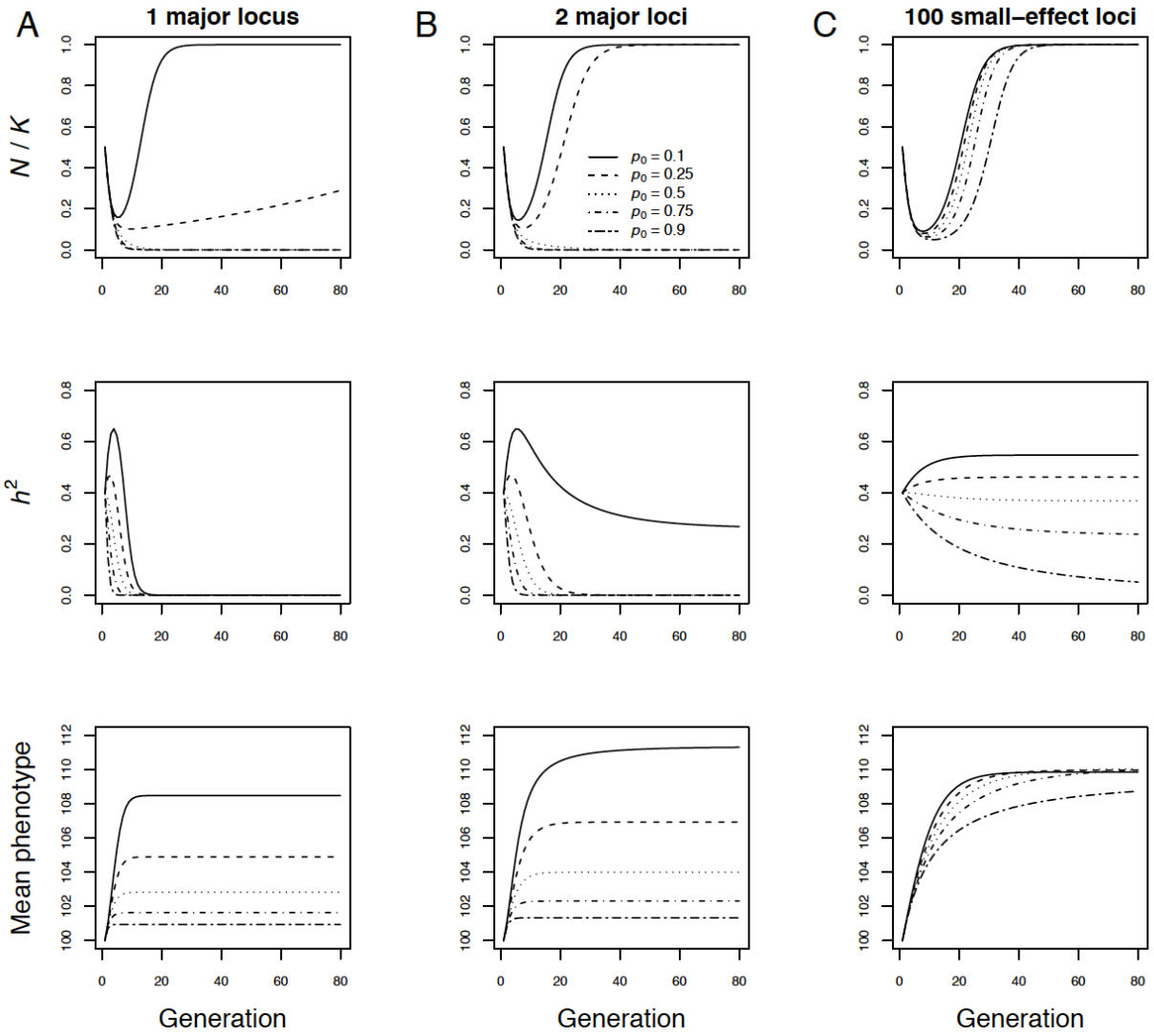

Figure S2. Deterministic predictions of evolutionary and demographic responses to directional selection in density-regulated populations with a single large-effect locus (**A**), two large-effect loci (**B**), and 100 small-effect loci (**C**) affecting a quantitative trait under directional selection after a sudden environmental change. The initial heritability was $h^2 = 0.4$ in all cases. Line types indicate the initial frequencies of the positively selected allele(s) conferring a larger phenotype. Initial population size was $K/2$.

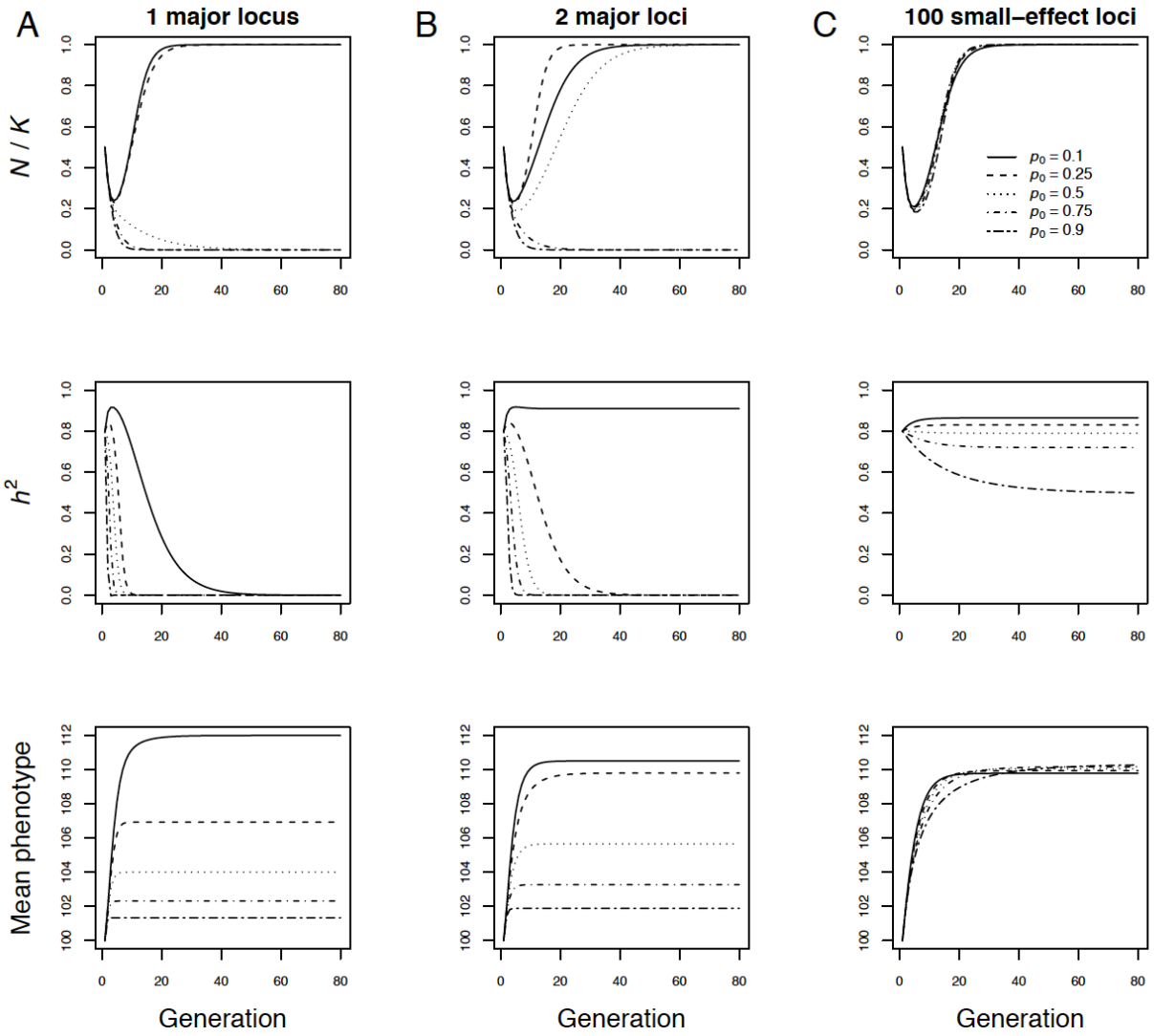

Figure S3. Deterministic predictions of evolutionary and demographic responses to directional selection in density-regulated populations with a single large-effect locus (**A**), two large-effect loci (**B**), and 100 small-effect loci (**C**) affecting a quantitative trait under directional selection after a sudden environmental change. The initial heritability was $h^2 = 0.8$ in all cases. Line types indicate the initial frequencies of the positively selected allele(s) conferring a larger phenotype. Initial population size was $K/2$.

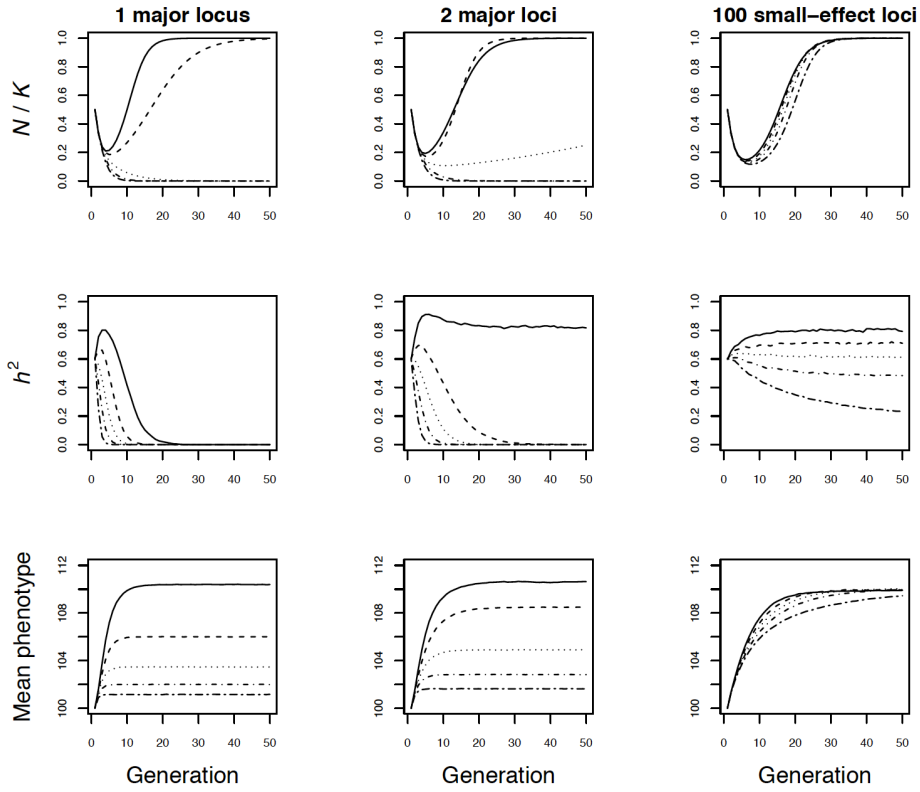

Figure S4. Evolutionary and demographic responses to a sudden change in the phenotypic optimum in density-regulated populations with a single large-effect locus (**A**), two large-effect loci (**B**), and 100 small-effect loci (**C**) affecting a quantitative trait under directional selection after a sudden environmental change. The lines in the first, second, and third rows show the mean population size, heritability, and mean phenotype across all 500 simulation repetitions versus time in generations. The initial heritability was $h^2 = 0.5$ in all cases. We varied the initial frequencies of the positively selected alleles conferring a larger phenotype from 0.1 to 0.9. Initial population size was $N_0 = 500$, and carrying capacity was $K = 1{,}000$ in all simulations. The lines show the mean of each parameter across 500 simulation repetitions. The mean h^2 and phenotype values shown were calculated across all populations with sizes $> N = 0$ each generation. The model used here is identical to that used to produce the data shown in Figure 1 in the main text, except here we simulated the distributions of individual genotypes and phenotypes to account for any selection-induced linkage disequilibrium and deviations from the normality in the phenotypic distribution. Specifically, each generation we simulated the genotypes, phenotypes, and mating among 50,000 pseudo individuals. The genotypes in the first generation were initialized using the assumed p_0. The phenotypes were simulated following the individual-based quantitative genetic model described in the main text. Offspring were assigned parents using weighted sampling (with the *sample* function in R), with the weights assigned based on phenotype using equation (1) in the main text. Population size in year t + 1 (N_{t+1}) was determined with equation (9) in the main text, with $\overline{w}_t$ replaced with the mean fitness among the 50,000 pseudo individuals in year t. This approach allowed us to precisely determine the expected distribution of individual fitness while accounting for any selection-induced linkage disequilibrium and non-normality in the phenotype distribution.

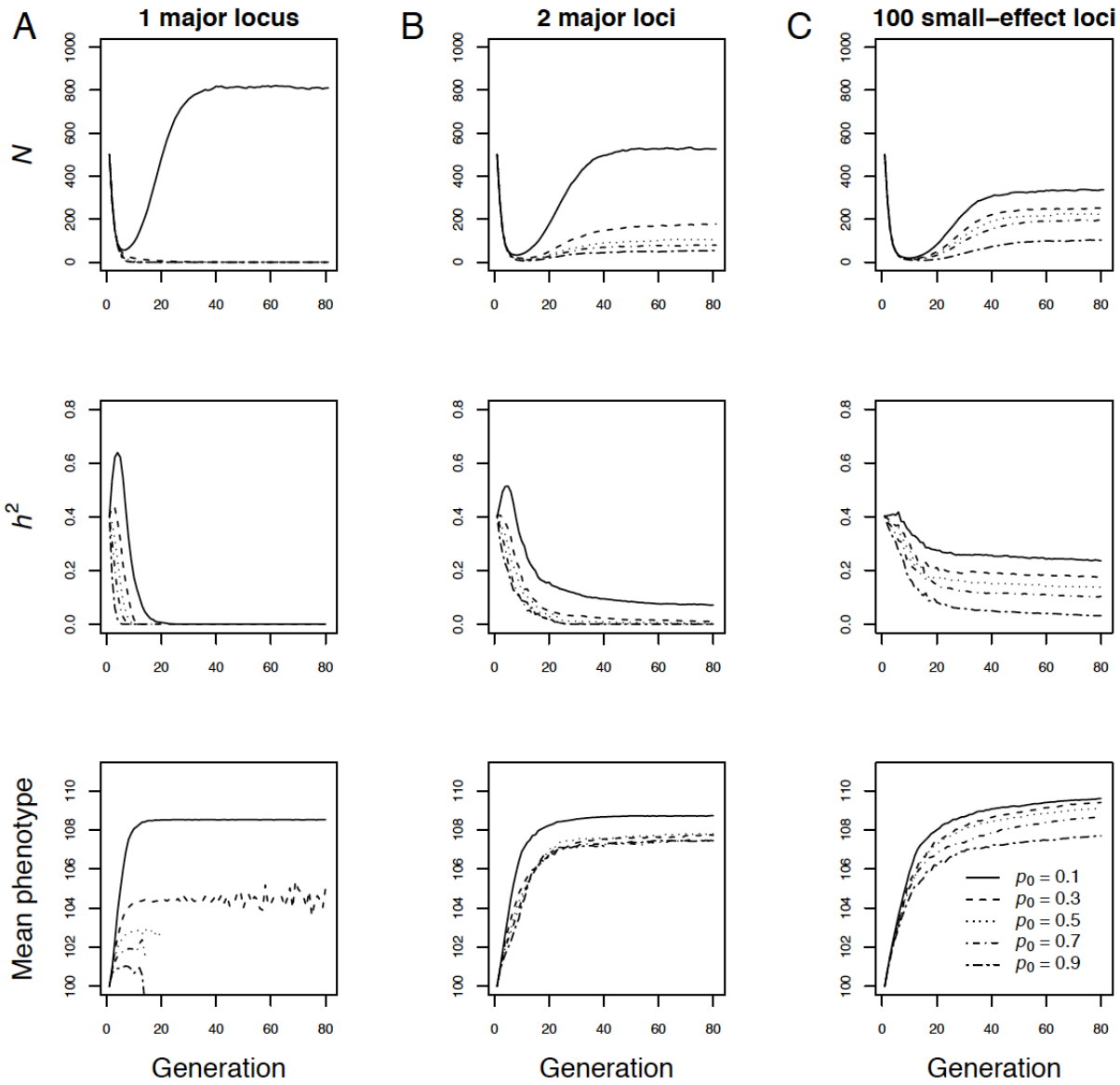

Figure S5. Individual-based simulations of evolutionary and demographic responses to directional selection in density-regulated populations with a single large-effect locus (**A**), two large-effect loci (**B**), and 100 small-effect loci (**C**) affecting a quantitative trait under directional selection after a sudden environmental change. The initial heritability was $h_0^2 = 0.4$ in all cases. Line types indicate the initial frequencies of the positively selected allele(s) conferring a larger phenotype. Initial population size was $N_0 = 500$, and varying capacity was $K = 1{,}000$. The extinction rates from these simulations are shown in Figure S6. The lines in the first, second, and third rows show the mean population size, heritability, and mean phenotype across all 500 simulation repetitions versus time in generations.

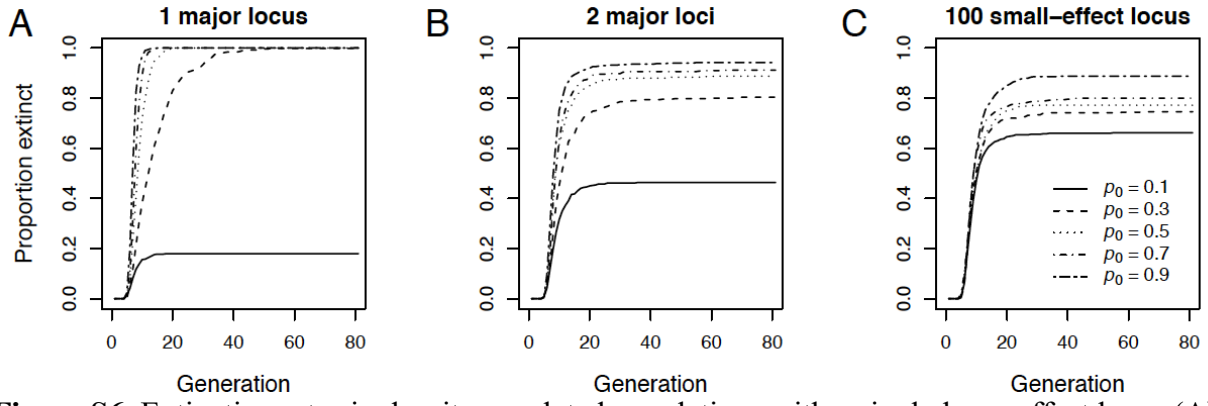

Figure S6. Extinction rates in density-regulated populations with a single large-effect locus (**A**), two large-effect loci (**B**), and 100 small-effect loci (**C**) affecting a quantitative trait under directional selection after a sudden environmental change. The initial heritability was $h_0^2 = 0.4$ in all cases. Line types indicate the initial frequencies of the positively selected allele(s) conferring a larger phenotype. Initial population size was $N_0 = 500$, and varying capacity was $K = 1{,}000$.

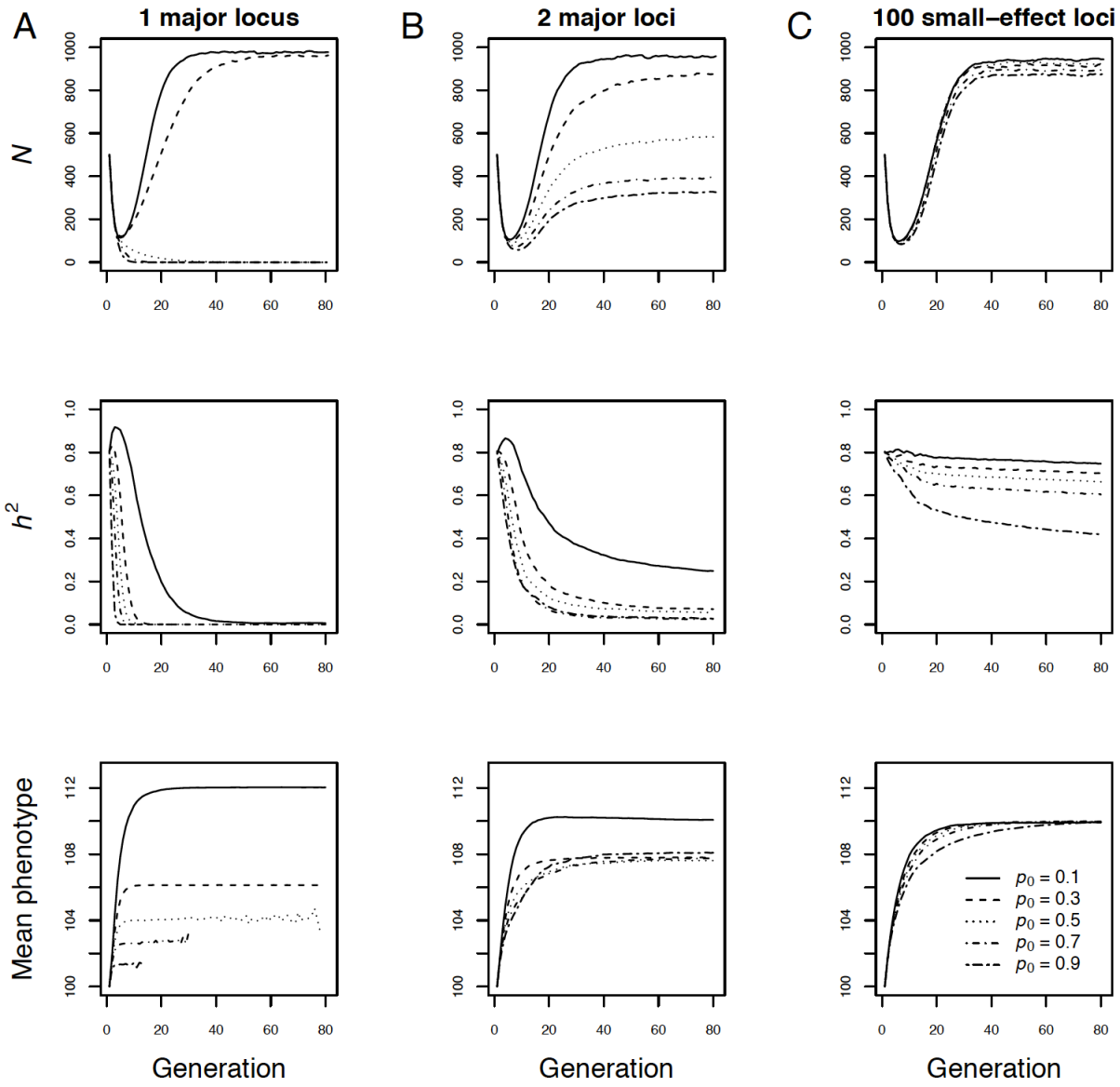

Figure S7. Individual-based simulations of evolutionary and demographic responses to directional selection in density-regulated populations with a single large-effect locus (**A**), two large-effect loci (**B**), and 100 small-effect loci (**C**) affecting a quantitative trait under directional selection after a sudden environmental change. The lines in the first, second, and third rows show the mean population size, heritability, and mean phenotype across all 500 simulation repetitions versus time in generations. The initial heritability was $h_0^2 = 0.8$ in all cases. Line types indicate the initial frequencies of the positively selected allele(s) conferring a larger phenotype. Initial population size was $N_0 = 500$, and varying capacity was $K = 1{,}000$. The extinction rates from these simulations are shown in Figure S8.

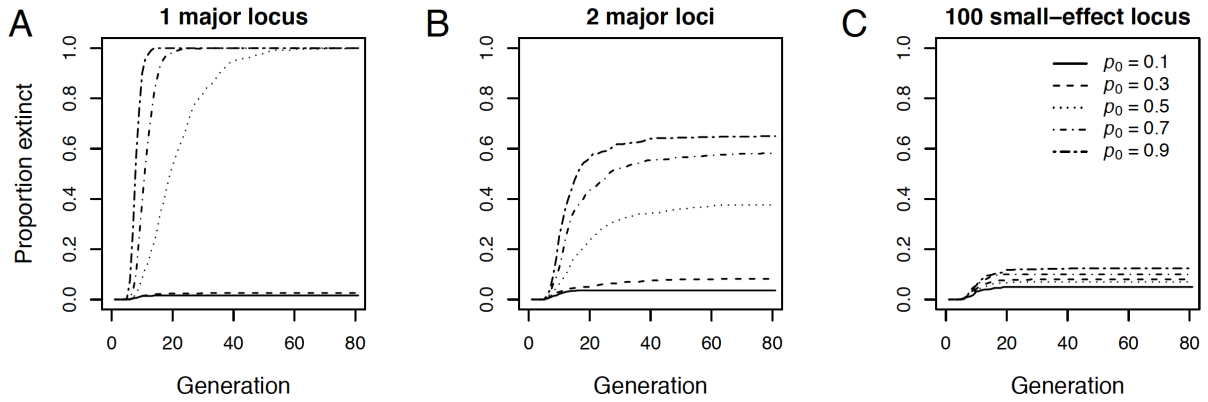

Figure S8. Extinction rates in density-regulated populations with a single large-effect locus (**A**), two large-effect loci (**B**), and 100 small-effect loci (**C**) affecting a quantitative trait under directional selection after a sudden environmental change. The initial heritability was $h_0^2 = 0.8$ in all cases. Line types indicate the initial frequencies of the positively selected allele(s) conferring a larger phenotype. Initial population size was $N_0 = 500$, and varying capacity was $K = 1{,}000$.

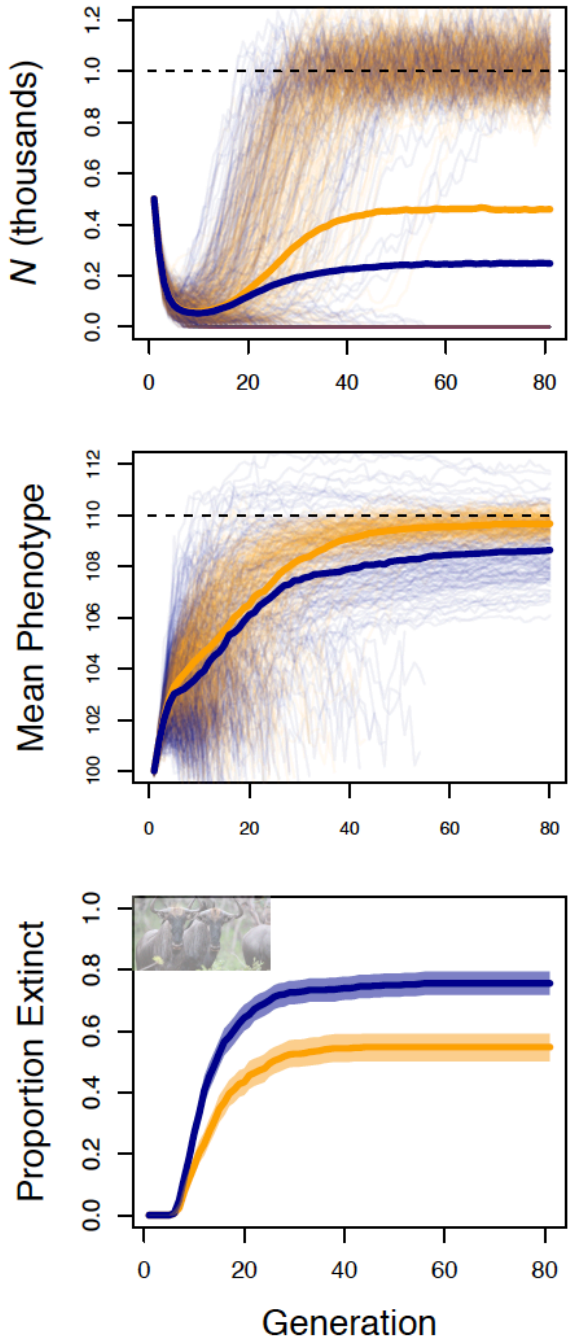

Figure S9. Effects of genetic architecture on phenotypic evolution and population dynamics in populations with an approximate large mammal life history and a low immigration rate (4 immigrants per generation) from a population with a constant phenotypic optimum of size = 100. Results from populations with a large-effect locus are shown in blue; populations where the selected trait was polygenic are in orange. Thin lines show the population size (top row) and mean phenotype (middle row) through time. Thick lines show the mean population size and phenotype across all 500 repetitions. The bottom panels show the proportion of extinct populations through time, with bootstrap 95% confidence intervals.

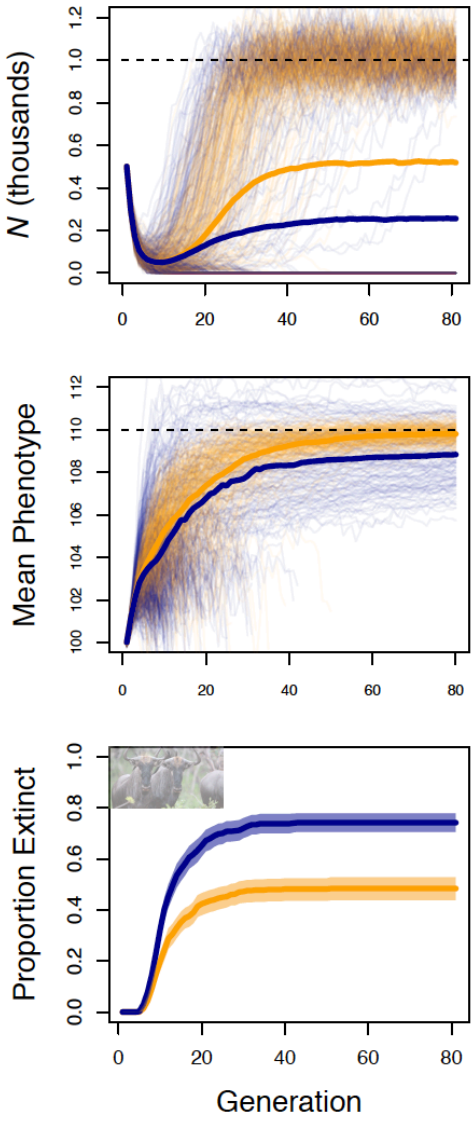

Figure S10. Effects of genetic architecture on phenotypic evolution and population dynamics in populations with an approximate large mammal life history and a high immigration rate (8 immigrants per generation) from a population with a constant phenotypic optimum of size = 100. Results from populations with a large-effect locus are shown in blue; populations where the selected trait was polygenic are in orange. Thin lines show the population size (top row) and mean phenotype (middle row) through time. Thick lines show the mean population size and phenotype across all 500 repetitions. The bottom panels show the proportion of extinct populations through time, with bootstrap 95% confidence intervals.

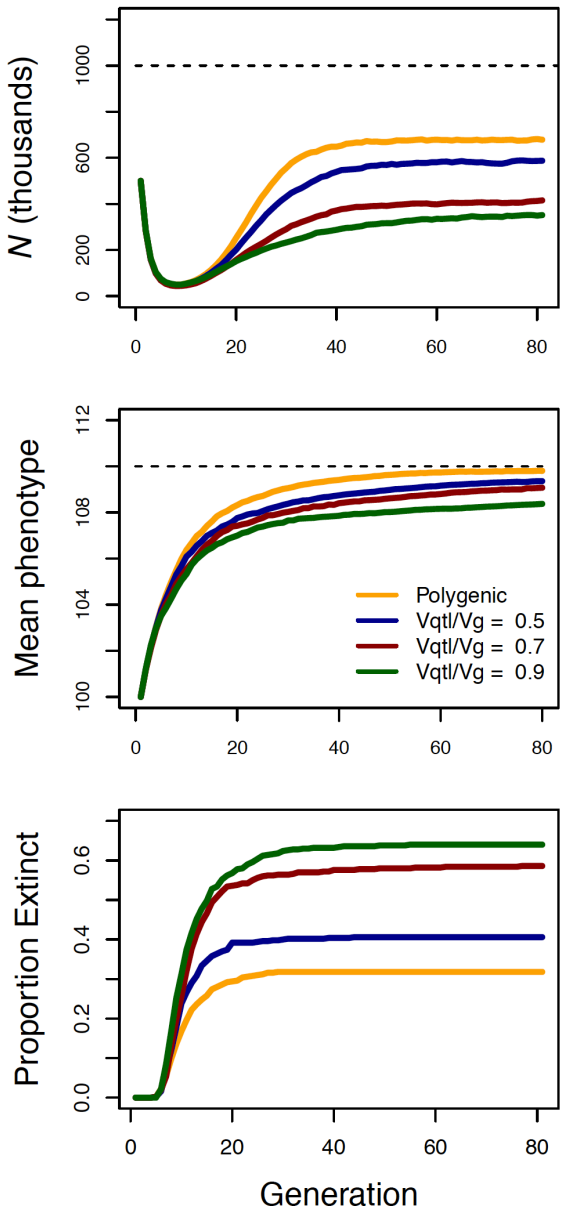

Figure S11. Effects of the effect size of large-effect loci on population dynamics.
The results are from simulations parameterized as in our simulations shown in Figure 3A, except here we varied the proportion of the genetic variance attributed to the large effect locus. Results from populations where a major locus was responsible for 90% (green), 70% (red), 50% (blue) of the additive genetic variance (V_G). Orange lines show results from populations where there selected trait was polygenic (no large-effect locus). The bottom panel shows the proportion of extinct populations though time.

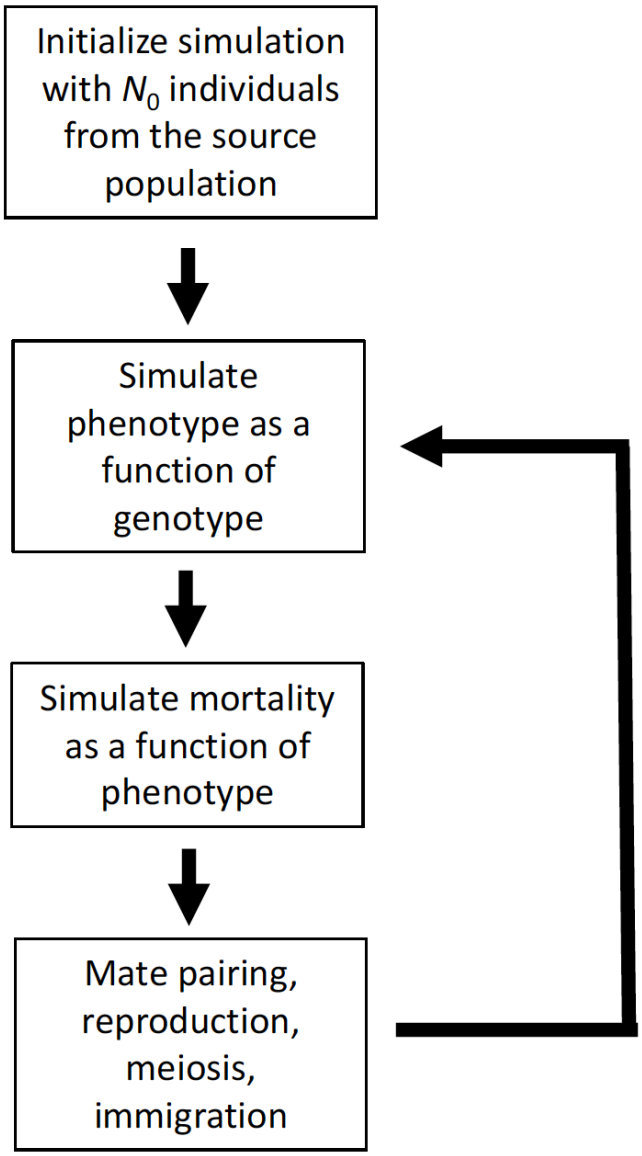

Fig. S12. Flowchart of the sequence of events in the simulation model. Details of each step in the simulation procedure are described in detail above in the Material and Methods.

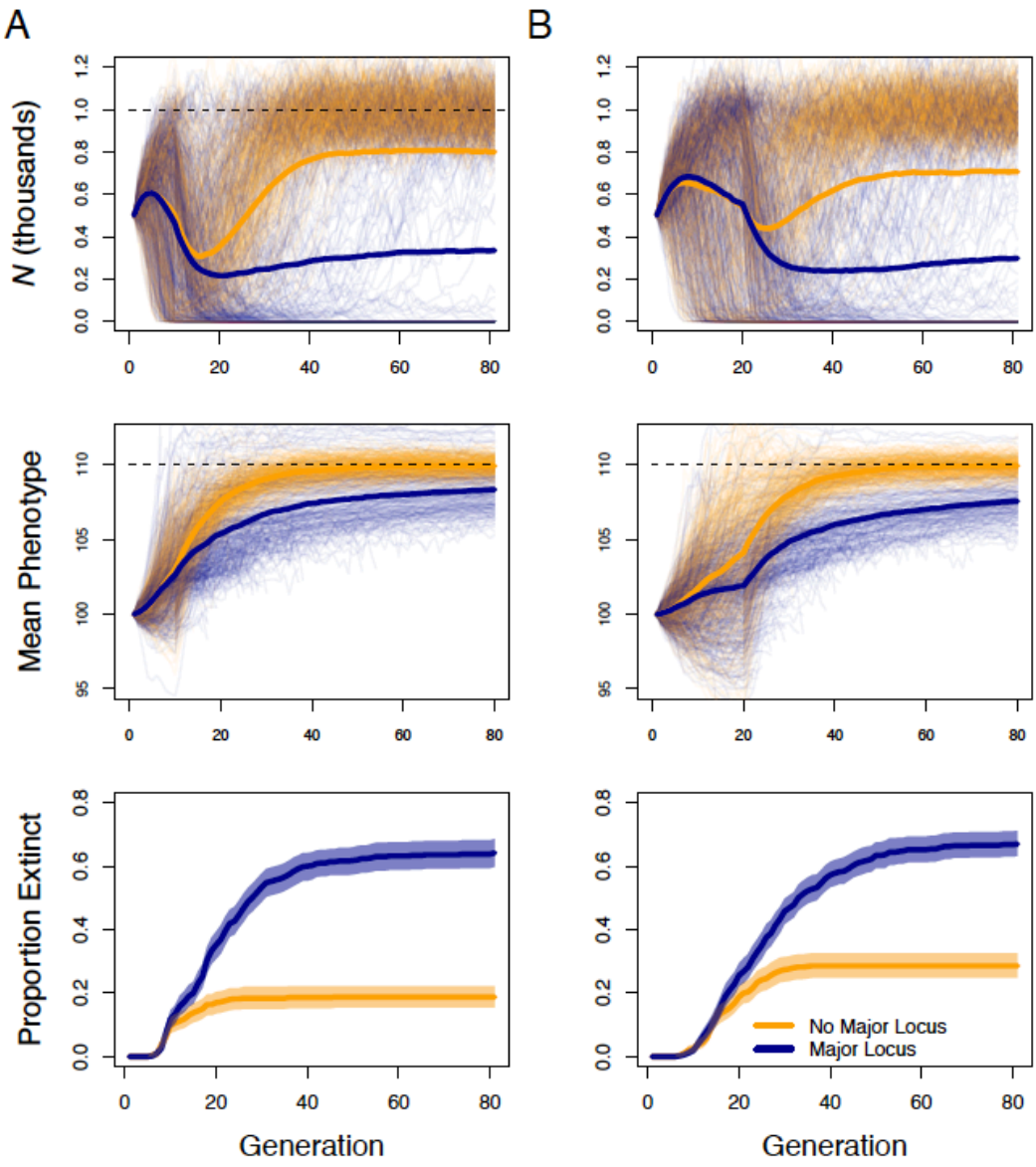

Figure S13. Effects of genetic architecture on phenotypic evolution and population dynamics in populations with a large mammal-like life history and with a stochastic linear increase in the optimum phenotype value with time. We ran simulations where the expected optimum phenotype increased linearly from 100 to 110 in either 10 (**A**) or 20 (**B**) generatiosn. Results from populations with a large-effect locus are shown in blue; populations where the selected trait was polygenic are in orange. Thin lines show the population size (top row) and mean phenotype (middle row) through time. Thick lines show the mean population size and phenotype across all 500 repetitions. The bottom panels show the proportion of extinct populations through time, with bootstrap 95% confidence intervals.

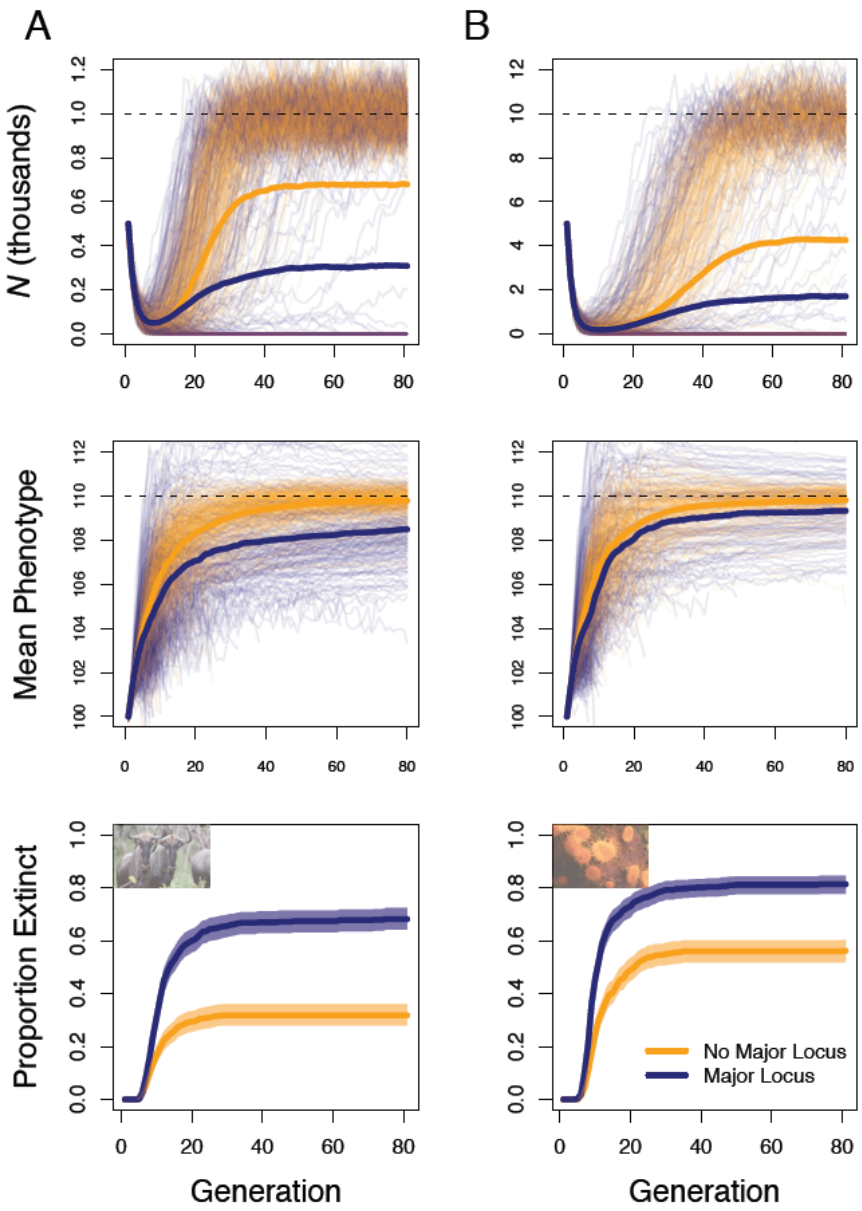

Figure S14. Effects of genetic architecture on phenotypic evolution and population dynamics with linkage in closed populations with life histories approximating large mammals (**A**), and corals (**B**). Results from populations with a large-effect locus are shown in blue; populations where the selected trait was polygenic are in orange. Thin lines show the population size (top row) and mean phenotype (middle row) through time. Thick lines show the mean population size across all simulation replicates. The bottom panels show the proportion of extinct populations through time, with bootstrap 95% confidence intervals.

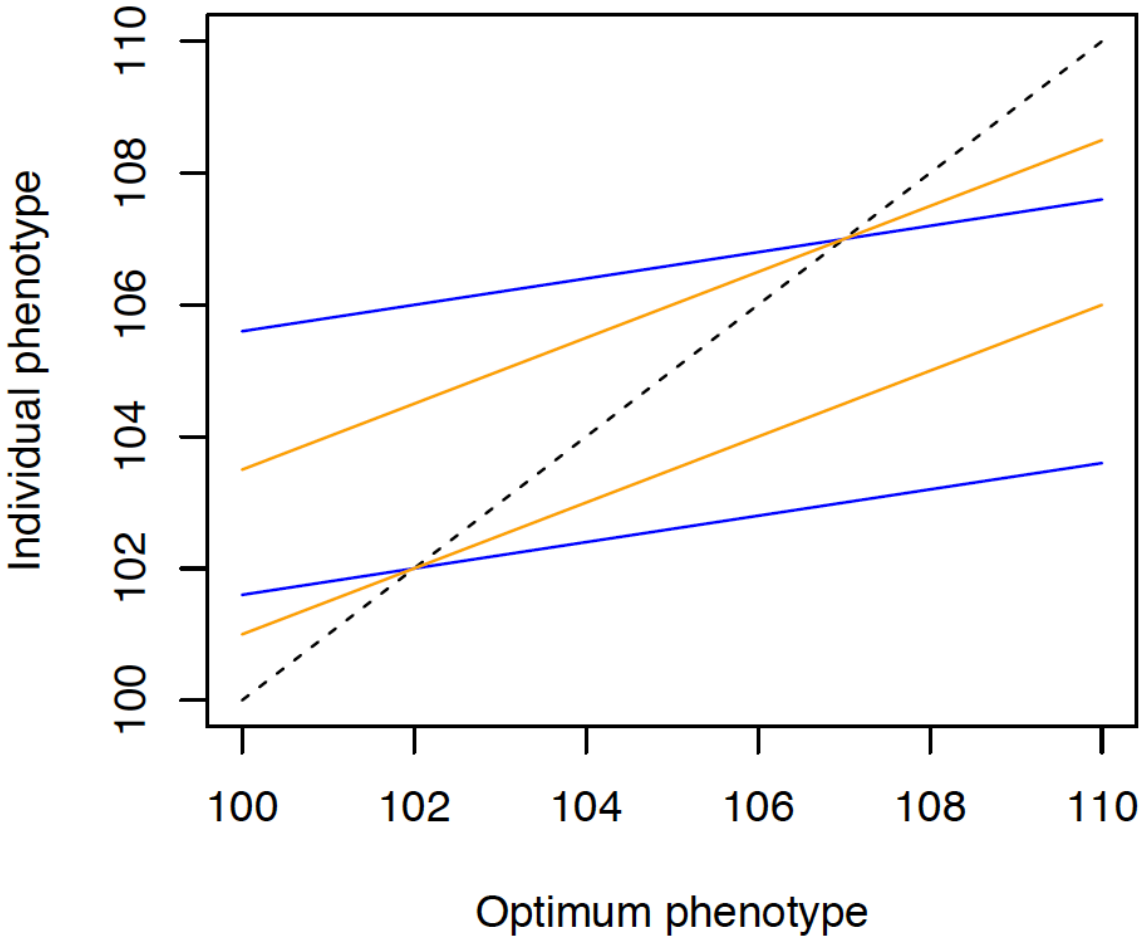

Figure S15. Model of plasticity shown as the individual phenotype plotted against the optimum phenotype. The dashed black line represents the case where individual phenotype equals the optimum phenotype. The expected phenotypes (i.e., ignoring random environmental effects) are shown for two individuals with breeding values of 102 and 107. The blue lines show the expected phenotypes with plasticity parameter $m = 0.2$, and the orange lines show the expected phenotypes with $m = 0.5$.

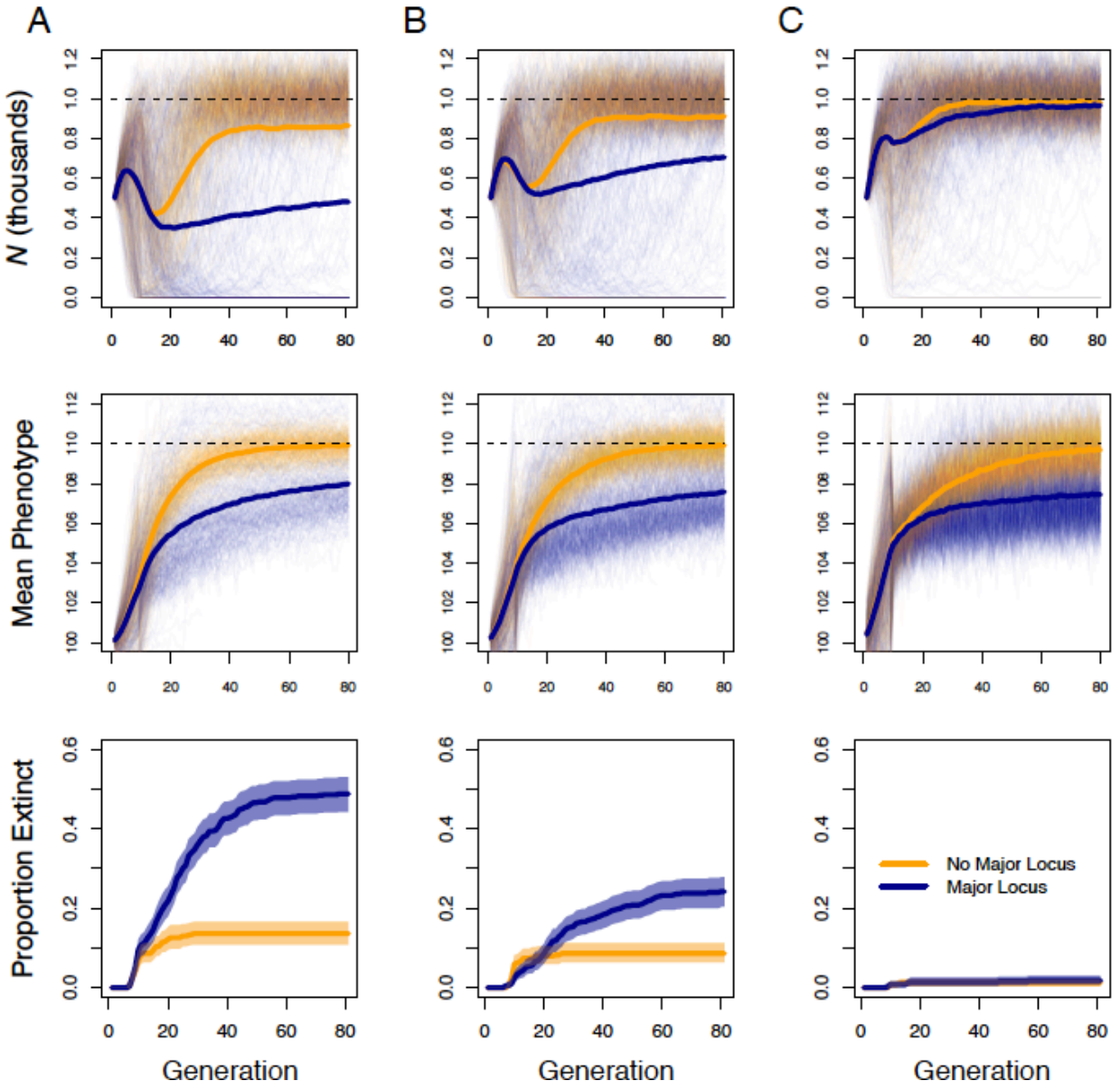

Figure S16. Effects of genetic architecture on phenotypic evolution and population dynamics in populations with life histories approximating large mammals and plasticity in the selected phenotype. Results are shown form simulation with the strength of selection set to $m = 0.1$ (**A**), $m = 0.1$ (**B**), $m = 0.4$ (**C**). Results from populations with a large-effect locus are shown in blue; populations where the selected trait was polygenic are in orange. Thin lines show the population size (top row) and mean phenotype (middle row) through time. Thick lines show the mean population size across all simulation replicates. The bottom panels show the proportion of extinct populations through time, with bootstrap 95% confidence intervals.

References

1 Yeaman, S. & Whitlock, M. C. The genetic architecture of adaptation under migration–selection balance. *Evolution: International Journal of Organic Evolution* **65**, 1897-1911 (2011).

2 Betancourt, A. J. & Presgraves, D. C. Linkage limits the power of natural selection in Drosophila. *Proceedings of the National Academy of Sciences* **99**, 13616-13620 (2002).

3 Nunney, L. Adapting to a changing environment: modeling the interaction of directional selection and plasticity. *Journal of Heredity* **107**, 15-24 (2015).